Volume 8
Number 40
28 October 2020
Pages 20735–21342

Journal of Materials Chemistry A

Materials for energy and sustainability

rsc.li/materials-a

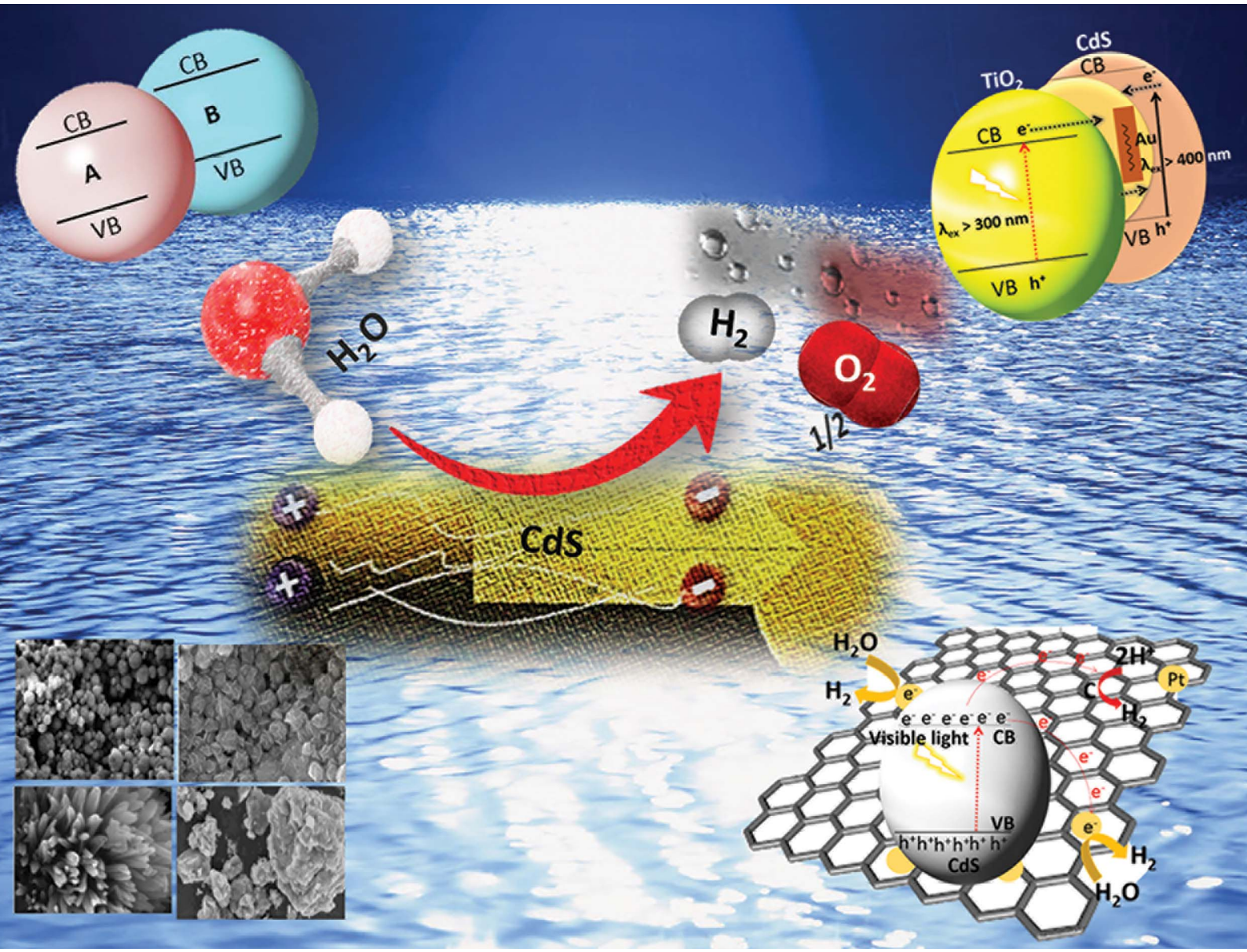

ISSN 2050-7488

ROYAL SOCIETY OF CHEMISTRY

REVIEW ARTICLE

Zia ur Rehman, C. Richard A. Catlow *et al.*

Recent developments and perspectives in CdS-based photocatalysts for water splitting

Journal of Materials Chemistry A

ROYAL SOCIETY OF CHEMISTRY

REVIEW

View Article Online
View Journal | View Issue

Cite this: J. Mater. Chem. A, 2020, 8, 20752

Recent developments and perspectives in CdS-based photocatalysts for water splitting

Jamal Abdul Nasir, [ac] Zia ur Rehman, *[a] Syed Niaz Ali Shah, [a] Azam Khan,[a] Ian S. Butler [b] and C. Richard A. Catlow *[cd]

Over the past few years, many approaches have been developed progressively to produce hydrogen (H_2) from water under solar light irradiation. This process of fuel production is clean, potentially cost-effective, and environment-friendly. At present, however, current technologies are unable to meet the industrial requirements because of high cost, low photoresponse, and insufficient catalytic performance. Among water splitting photocatalysts, CdS is considered to be an interesting and important material owing to its low cost, prominent catalytic activity, high absorption in the visible spectrum, and the suitable positions of its conduction (CB) and valence (VB) bands. There are, however, some associated problems such as the rapid recombination of photogenerated electron–hole pairs and photocorrosion that have severely hampered its practical usage. The efficient conversion of water to H_2 depends on the extent to which the charge carriers, especially the electrons, are first generated and then have sufficient life-time for their effective utilization. This review highlights work over the past several years to improve the photocatalytic efficiency and stability of CdS for H_2 production from water.

Received 12th June 2020
Accepted 12th August 2020

DOI: 10.1039/d0ta05834c

rsc.li/materials-a

[a]Department of Chemistry, Quaid-i-Azam University, Islamabad, 45320, Pakistan. E-mail: zrehman@qau.edu.pk; hafizqau@yahoo.com

[b]Department of Chemistry, McGill University, 801 Sherbrooke St. West, Montreal, Quebec, H3A 0B8, Canada

[c]Department of Chemistry, Kathleen Lonsdale Materials Chemistry, University College London, 20 Gordon Street, London WC1H 0AJ, UK. E-mail: c.r.a.catlow@ucl.ac.uk

[d]School of Chemistry, Cardiff University, Park Place, Cardiff, CF10 3AT, UK

Jamal Abdul Nasir received his MSc and MPhil degree in Inorganic/Analytical Chemistry from Quaid-i-Azam University Islamabad Pakistan in 2014 and 2016 respectively. He joined the same institute as a PhD student in September 2016 and completed his coursework and research under the supervision of Dr Zia ur Rehman. He has published more than 8 research articles in various journals of international repute. Currently, he is a part of Prof. Richard's group at University College London. He has a decent research background in material science, especially in photocatalysis and holds a keen interest in the area of QM/MM calculation for zeolite-based materials to investigate NOx decomposition, reaction mechanism, and designing photoactive materials for H_2 production and CO_2 reduction.

Dr Zia ur Rehman is working as a Tenured Associate Professor at Quaid-i-Azam University Islamabad, Pakistan. His group is involved in the synthesis of new materials for biomedical, clean energy, and environmental applications. He has published 110 research articles in various journals of international repute, and co-author of a book entitled "DNA Binding and DNA Extraction: Methods, Applications, and Limitations". In his short academic carrier, 6 PhDs and 38 MPhil students obtained their degrees in his direction. His teaching and research efforts have been recognized by the Dr Abus Salam Award from TWAS and Pakistan Academy of Sciences (PAS), Dr Atta-ur-Rahman Gold Medal (PAS), and CSP Gold Medal (The Chemical Society of Pakistan). He is a young member of the PAS and International Committee Member of ACCC.

Introduction

Energy is an essential part of economic activity. Today, most energy is produced from fossil fuel combustion, which as is well-known results in the emission of carbon dioxide, one of the major greenhouse gases responsible for climate change.[1–4] Moreover, the amount of available fossil fuel is finite and is continuing to be depleted. The total worldwide power demand,

Dr Syed Niaz Ali Shah did his postdoc (2017/10 to 2019/10) from Tsinghua University, Beijing, China. He got his PhD degree in analytical chemistry from the Department of Chemistry, Tsinghua University, Beijing, China, in July 2017. He got his MPhil degree in inorganic/analytical chemistry from the Department of Chemistry, Quaid-i-Azam University, Islamabad, Pakistan, in 2014, and Master's degree in analytical chemistry from the Institute of Chemical Sciences, University of Peshawar, Pakistan, in 2011. His research interests mainly focus on chemiluminescent nanomaterials and sensors. He is the author of more than 18 peer-reviewed articles.

Dr Azam Khan received his MPhil degree in Inorganic Chemistry from Hazara University Mansehra Pakistan in 2010. He completed a PhD in Inorganic/Analytical Chemistry under the supervision of Dr Zia ur Rehman at the Department of Chemistry Quaid-i-azam University Islamabad, Pakistan. His current research is focused on the design and synthesis of metal sulfide nanoparticles for energy and environmental applications. He has published more than 15 articles in various scientific areas.

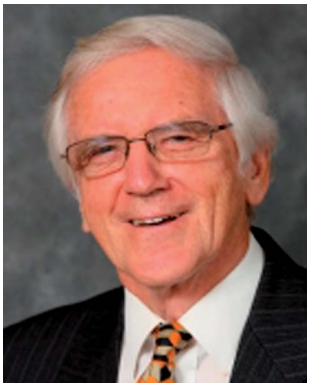

Professor Ian S. Butler was educated in U.K. at the University of Bristol and, following two years as a Fulbright postdoctoral scholar in the U.S.A, he joined the faculty in the Department of Chemistry at McGill University in 1966. He has served as Department Chair and Associate Vice-Principal (Research). He is an Honorary Member of the Spectroscopy Society of Canada, a Fellow of both the Chemical Institute of Canada and the Royal Society of Chemistry (U.K.). He has supervised over 200 researchers, resulting in the co-authorship of about 560 publications. He has also published several text books on General Chemistry, Inorganic Chemistry and Erbium. His honours include the Gerhard Herzberg Award for Excellence in Spectroscopy and the David Thomson Award for Excellence in Graduate Teaching and Supervision. His current research focuses on structural changes induced by high pressures and variable temperatures, bioinorganic chemistry, biomass conversion, mechanochemistry and art forensics. He has been married to his wife Pamela, a former dancer with American Ballet Theatre and a Professor of Political Science, for 55 years and they have four children and 15 grandchildren.

Professor C. Richard A. Catlow obtained his doctorate from the University of Oxford and subsequently held academic appointments at University College London, Keele University, the Daresbury Laboratory, and the Royal Institution (RI). He was made director of the Davy-Faraday Research Laboratory (DFRL) in 1998, a position that he held until 2007. In 2002, he was appointed Head of the chemistry department at UCL, becoming the first person to lead the UCL chemistry department and the DFRL at the same time. Five years later, he left the RI to become full-time at UCL, where he was named Dean of Science. He is also Vice-President and Foreign Secretary of the Royal Society – the Academy of Science of the UK and the Commonwealth. His research concentrates on computational chemistry and materials sciences and has published over 1000 research articles in this field. He currently has a joint professorial position with UCL and Cardiff University. His research interests are in the field of the chemistry of complex materials, including those for applications in catalytic and energy applications, investigated by a combination of computational and experimental techniques.

however, which was 17 TW in 2010, is expected to rise to 27 TW by 2040.[5] It is widely accepted that it is essential to solve future energy crises and current environmental threats by identifying a clean, safe, and renewable energy source. Solar energy technologies are attractive alternatives to fossil fuels as the total solar energy received by the Earth's surface in an hour is enough to meet the annual global energy demand.[6–8] The challenge of energy storage and integration into the current power grid can, however, be a hindrance to the implementation of these technologies.[9] An alternative promising approach is provided by photocatalytic water splitting for the production of H_2.[10,11] However, a suitable photocatalyst needs to be efficient, stable, and to consist of Earth-abundant elements.[12] Many attempts have been made to develop such a catalyst from non-precious, Earth-abundant elements[13,14] and considerable progress has been made, but the search is still underway.

Amongst the earliest research on photoelectrochemistry was the work of Brattain,[15] who studied germanium electrolyte junctions. This work was quickly followed by that of other groups.[16,17] Later, Bard *et al.*[18] demonstrated the photocatalytic behaviour of suspended semiconductor (SC) nanoparticles (NPs) and Nozik *et al.*[19] explored the idea of photochemical diodes. The concept of water splitting through photoelectrochemistry was first established in 1972 by Honda and Fujishima using titania electrodes.[20,21] Since then, various SC photoelectrodes and photocatalysts have been examined.[22–25] Photochemical water splitting reactions require chemical energy from the direct sunlight source that involves a large positive change in Gibbs free energy (an endoergic reaction, $\approx$237 kJ mol^{-1}). This process is similar to photosynthetic reactions in plants[26] and is thus often regarded as artificial photosynthesis (eqn (1)). The absorption of light by a photocatalyst is required to produce a large enough potential to perform water splitting; moreover, the electron–hole life-time in this context is very important and should be sufficient for the redox reactions to proceed.[27]

$$H_2O \rightarrow \frac{1}{2}O_2(g) + H_2(g);\ \Delta G = +237\ \text{kJ mol}^{-1} \quad (1)$$

The reaction needs a potential of 1.23 eV and the band gap of the SC in this context should, therefore, be greater than 1.23 eV (<1000 nm) and less than 3.0 eV (>400 nm) so that it can be operated in the UV/visible region.

Recently, two primary approaches have been applied to establish an effective photocatalytic water splitting system[28] (Fig. 1). In one approach, a single photocatalyst is used to drive the overall process. In this case, the SC must have a suitable band gap to harvest visible light and a sufficient thermodynamic potential for the water-splitting redox reactions. As a consequence of these restrictions, the number of efficient and stable photocatalysts for one-step water splitting is limited.[29,30] In an alternative approach, two different photocatalysts are used and a two-step excitation mechanism is followed.[18] This idea was taken from heterojunction[31] and Z-scheme[32–35] processes (like natural photosynthesis). The formation of a heterojunction between two photocatalysts allows charges to be transferred from one photocatalyst to another, thereby enhancing the life-time of the photogenerated charges. Similarly, the Z-scheme has many advantages over a one-step mechanism as two different SCs are combined with the introduction of a redox mediator species [electron donor/acceptor (A/D) pair], which acts as a shuttle between the two SCs.[36] The separation of the gases produced (H_2 and O_2) is also easier in this case. An advantage of this approach is that an SC with either an oxidation potential or a reduction potential sufficient to effect water splitting can be used as a half-reaction in a two-step process.[37,38]

Since the initial breakthrough in the splitting of water on *n*-TiO_2 electrodes (photoelectrochemically),[20] extensive work has been conducted on TiO_2-based catalysts.[39–41] Unfortunately, TiO_2 has a band gap energy of about 3.0–3.2 eV and absorbs UV light, <400 nm,[42] which hampers its use as a photocatalyst, because the solar spectrum contains only 3–4% of UV light. Consequently, there is an urgent need to develop a SC material that can harvest the copious amount of visible light (43%) in the solar spectrum. Additionally, photocatalysts for water oxidation should have a suitable redox potential for the CB and VB levels at neutral pH, together with a narrower band gap (<3.1 eV) capable of absorbing visible light irradiation.[28] In this context, the location of the VB of the SC should be sufficiently positive to oxidize the water molecule O_2/H_2O (1.23 V *vs.* NHE) and the CB should be negative enough for the reduction of a proton (H^+/H_2 0 V *vs.* NHE).[43] Among the visible-responsive photocatalysts,[44] much work has focused on CdS, because of its low cost, appropriate band gap, and electron affinity that best fit the visible light absorption spectrum.[45–49] The photocatalytic properties of CdS are somewhat limited though, because of several issues such as (i) photocorrosion and (ii) aggregation of CdS NPs during photocatalysis, which causes a large decrease in surface area and loss of active-sites. To mitigate the photocorrosion and to increase the overall efficiency of CdS, common sacrificial reagents such as Na_2S/Na_2SO_3,[50] ethanol,[51] formic acid,[52] and other organic and inorganic reagents are used.[10,53–55] The benefits and detriments of these sacrificial agents will be discussed later. Other approaches for enhancing the activity of CdS include the control of the particle sizes[56] (*i.e.*, preparation of quantum-sized particles), tuning the morphology of the NPs,[57] loading of co-catalysts[58] (*i.e.*, doping with noble and non-noble metals) and the combination of CdS with other SC materials to form mixed photocatalysts.[59] Among these, the combination of different band gap SCs and the loading of suitable co-catalysts onto CdS are effective approaches for enhancing photocatalytic activity.[60–62] More generally, the optimization of any material for photocatalytic activity requires that the following three fundamental factors be considered: (i) the absorption of light for generation of charges, (ii) the separation of the charges especially electrons and their effective transportation and (iii) the utilization of electrons for overall water splitting.

To improve the light absorption of wide-band gap SC materials, band gap engineering,[63–67] surface plasmonic enhancement, doping with narrow-band gap SC materials,[68–70] dye sensitization,[71,72] and disorder engineering[73,74] have been employed. To avoid charge recombination and assist charge

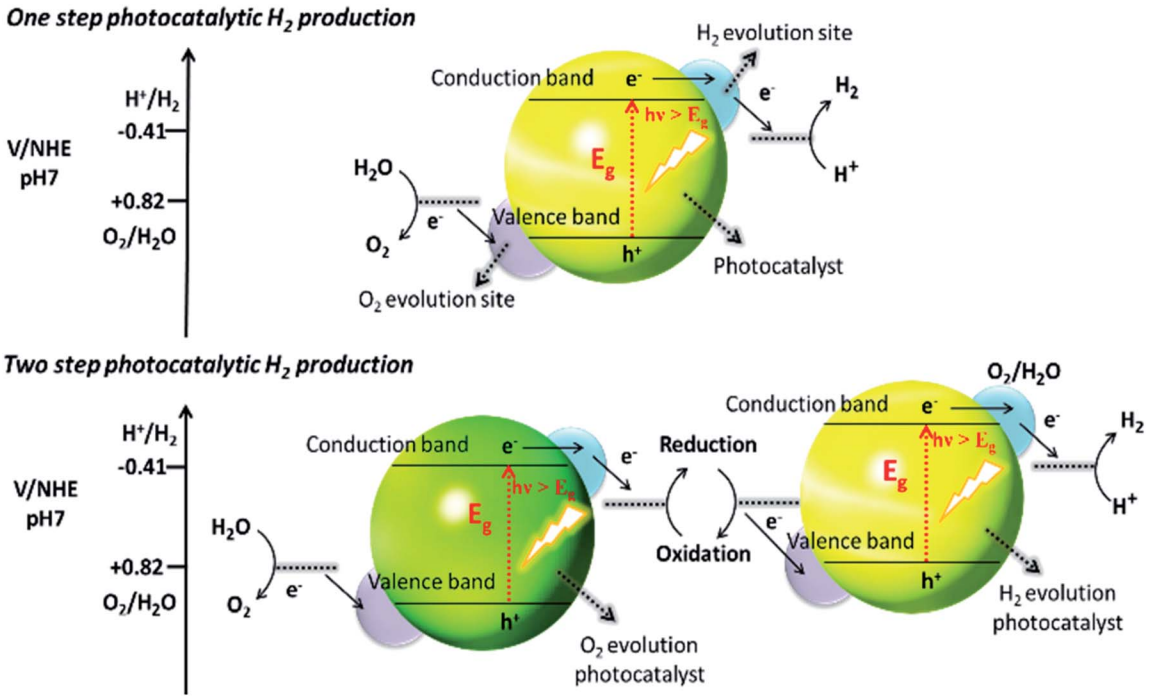

Fig. 1 Schematic illustration of photocatalytic water splitting by one-step and two-step photoexcitation system. Reproduced with permission from ref. 28.

transport, various morphologies of SC materials have been tuned on a nanoscale by the formation of nanospheres, nanorods, quantum dots, nanotubes and nanosheets.[49,70,75,76] In addition to morphology tuning, co-catalyst incorporation, heterojunction creation, and Z-scheme developments have also proved highly effective for improving this second step. The third factor is encouraged by surface functionalization and by tailoring the reaction pathway through the use of sacrificial reagents. Co-catalysts play a dual role: (i) preventing recombination and (ii) acting as active sites either for activation of water molecules or for the reduction of protons. In the co-catalyst strategy, holes or electrons are scavenged by the co-catalysts once they are generated within the photocatalyst. Oxidative co-catalysts[77] scavenge holes, while reductive co-catalysts[78] trap electrons. By introducing an oxidative co-catalyst, such as Co^{II}, not only is it possible to scavenge holes and hinder the recombination process but also it can provide an opportunity for the possible utilization of electrons.[26,28,59,79–83]

In the context of these challenges and approaches, the remainder of this review summarises recent developments in the study of CdS-based photocatalysts used for water splitting and considers the likely future development of the field; and we will consider CdS-based systems in the broader context of the field of water splitting by photocatalysts.

CdS as a photocatalyst: fundamentals and challenges

Visible-light-driven photocatalysts that are capable of the efficient production of H_2 have good light absorption capacity and sufficiently negative flat band potentials. Widely investigated materials include $TiO_2Fe_2O_3$, WO_3,[84] and the other materials referred to in Fig. 2, but especially CdS, which is one of the most widely investigated photocatalysts used in water splitting and in several other processes because of its suitable band gap of around 2.4 eV. This band gap is sufficiently negative for proton reduction (H_2O/H_2), as shown in Fig. 2.[85] The band gap, of course, satisfies the thermodynamic requirement.[86] Various other aspects, as noted above, affect the photocatalytic process, such as charge separation, and transportation, and life-time, over-potentials, and the pH of the system. Associated issues, such as photocorrosion and particle aggregation, also limit the photocatalytic activity of CdS.

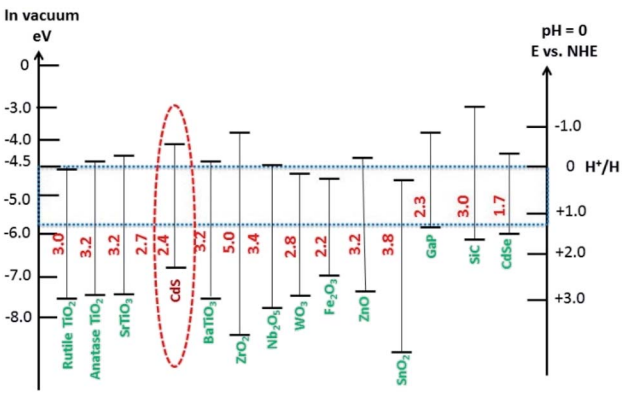

Fig. 2 The band gap positions for CdS and other SCs relative to the redox potential of water.

Photocorrosion is a common phenomenon and one of the greatest challenges with CdS or CdS-based photocatalysts, which hinders their practical use on an industrial scale. This phenomenon arises when (i) the sulfur ions are attacked by photogenerated holes and are oxidized into elemental sulphur; (ii) the photogenerated holes lead to the anodic corrosion under irradiation; and (iii) the defects created on the CdS surface during photocatalysis facilitate redox reactions on the surface under aerobic conditions.[87] Photocorrosion has greatly limited the use of CdS,[88] but fortunately, it can be inhibited and the stability of CdS can be improved by incorporation of an oxide layer,[89] combining it with other materials (microporous and mesoporous),[51,90] coupling with metallic/non-metallic catalysts,[91,92] coating its surface,[93] heterojunction formation,[94] morphology tuning,[95] cocatalysts incorporation,[96] and the addition of sacrificial reagents.[97] Meissner *et al.* have incorporated various catalysts such as Ru_2O and Rh_2O_3 into CdS-monograin membranes to obtain more insight into water cleavage by suppressing the corrosion of the CdS nanocatalyst.[98]

According to previous reports, corrosion of CdS has been observed mostly in an acidic medium.[99] The reaction media have a profound effect on the photocatalytic activity of CdS. To tailor the reaction pathway, increasing the pH of the media results in holes transferring from the photocatalyst to the scavenger (*i.e.* ethanol) as reported by Simon *et al.*[78] In basic media, the release and transfer of holes operates as a shuttle and the redox couple of $^{\bullet}OH/^{-}OH$ affords electrons for proton reduction, while the hydroxyl anions are regenerated through water dissociation. In general, the process of hole scavenging from the VB of photocatalyst to the sacrificial electron donor is mainly favorable at high pH. On the other hand, operating the photoreaction in acid media not only makes hole transportation difficult but also causes the corrosion of photocatalyst.

As the pH of the reaction media affects the cleavage of a water molecule as well the stability of photocatalyst, such studies should be carried out in basic media to avoid corrosion as well as to assist water splitting. Similarly, Torimoto *et al.* reported that metal chalcogenides such as CdS are photocorroded.[100] Also, Hu *et al.* showed that the photocorrosion in CdS based photocatalysts of sulphide ions by photo generated holes makes CdS unstable for photocatalysis.[101] Similarly, other reports showed that photogenerated holes attack sulfide ions accompanied by leaching of the toxic Cd^{2+} ions.[26,102] The concentration effect of Cd^{2+} ions[103] and the kinetics during photocorrosion of CdS have been also studied in this regard using *in situ* Raman spectroscopy.[104] A significant effect on photocorrosion of different environments (air and argon) was noted and the catalytic performance was changed in the two atmospheres, but the structural characteristics remained the same. Furthermore, the rate of H_2 formation in an argon environment was much higher than in air. The decrease in activity was attributed to the "lattice stress "of CdS in air (oxygen environment). This term is related to some surface substitution of S^{2-} ions by O^{2-} ions in the CdS lattice. The increase in the lattice stress during photoreaction could be due to the rapid interaction between CdS and the adsorbed O_2 leading to a decrease in activity. Furthermore, it is anticipated that the increase in strain and lattice stress is the initial sign of photocorrosion in CdS based photocatalyst, which, however, can be difficult to investigate through traditional techniques such as XRD. It is, therefore, necessary to develop a new CdS-based photocatalyst to overcome these difficulties, as will now be discussed.

Pure SC NPs like those of CdS are prone to surface damage as discussed above. Some surface modification of the CdS nanocatalyst is therefore needed,[105] which may, however, appreciably change the photocatalytic, chemical, and optical properties.[106] Numerous methods of modification have, moreover, been reported to tune the catalytic properties of CdS, such as noble metal loading,[107–109] ion doping,[110] SC composite formation,[111] and metal ion-implantation.[112]

Although, CdS has an excellent ability to absorb visible light, however, the extension of its absorption into the entire visible range and in some cases to the IR region can be achieved by some modification such as surface plasmonic enhancement. Moreover, modification has advantages such as suppressing electron–hole recombination, enhancing photostability, and creating new sites on the surface, which may lead to the creation of a new layer, thus improving the selectivity and overall efficiency of the photocatalyst, as has been reported for composites such as PbS/CdS[113] colloidal nanocrystals, ZnSe/CdS core–shell,[114,115] CdS/HgS/CdS quantum dot[116] and co-sensitized CdS/CdSe quantum dots.[117,118] In addition, the surface modification of a nano-chalcogenide is often achieved by the incorporation of metal ions onto the surface of NPs, as reported for CdS, *e.g.*, Mn,[119,120] Ag,[121,122] Zn,[123] Hg,[124] Ni,[78] *etc.* Electron utilization can be encouraged by surface functionalization and by tailoring the reaction pathway through the use of sacrificial reagents to enhance the water splitting reaction.

These and other challenges will be reviewed further in later sections. Meanwhile, in the next section, we address in greater detail the fundamental issues of charge generation and lifetimes.

Charge generation in CdS

Electron generation is the initial step in a photocatalytic H_2 production process and the extent and ability to reduce the desired species by the generated electrons are crucial factors in the H_2 evolution reaction (HER). The range of energy (300–2500 nm) supplied by the sun, comprises ~52% near infrared (>760 nm), ~43% visible (400 to 760 nm), and 3–4% ultraviolet (<400 nm) light. A photocatalyst with a narrow band gap has a good spectral response capturing photons with an energy corresponding to its band gap. As stated earlier, CdS, a narrow band gap SC, harvests nearly ~38% of the visible spectrum. As noted, efforts have been made to extend the absorption of the CdS up to the full visible range and the IR region. Two different approaches can be used to widen the spectral response of photocatalysts: self-modification and extra-modification. Self-modification refers to modifying a photocatalysts itself through structural defects and surface modification, while extra-modification means adding some additional material. Enhancing the spectral response through self-modification

might increase the chances of recombination and hence, would not be a suitable approach for CdS-like photocatalysts, as it already has a narrow band gap. Moreover, narrowing the band gap through self-modification causes a reduction of the CB, which weakens the reduction capacity of the photogenerated electrons. Therefore, many attempts have been made to widen the spectral response without decreasing the band gap of CdS by extra-modification. For example, the introduction of foreign light-harvesting materials is an effective method of modifying a CdS photocatalyst. However, the light blockage may occur on the surface of the catalyst due to foreign light-harvesting materials, and this effect should be taken into consideration. A more detailed discussion follows in the next section.

Modification of a narrow-band gap SC

The combination of photocatalysts for the purpose of the enhanced spectral response is an obvious way of extending the working spectrum. To acquire a broad spectral response, the wide band SCs are primarily co-sensitized by narrow band SCs such as CdS, CdTe, CdSe, PbS, which mainly serve as sensitizers in place of dye molecules. Among these, CdS is considered one of the most promising contenders owing to its broadly tuneable band gap and is, therefore, typically used to sensitize the wide band SCs in order to harvest the visible light irradiation, Wang *et al.* have used CdS with a double-sized incorporated CdSe nanohybrid co-sensitized with ZnO nanowires for photochemical H_2 production.[125] To develop this double-sided design, the thick ZnO nanowires were doped onto the indium tin oxide (ITO) substrate to which CdS and CdSe QDs were sensitized on each side (Fig. 3a). As a result, the photoanode displayed good absorption over almost the entire spectrum of the visible region, with an excellent incident-photon-to-current-conversion efficiency (IPCE) of ~45% (at 0 V *vs.* Ag/AgCl). Besides, the direct interaction between the quantum dot and the nanowire in the double-sided architecture makes it a promising system for effective charge collection as compared to a co-sensitized single-sided layer. Commensurate with this study, a different strategy was adopted by Vuong *et al.*, who prepared ZnO nanorods, sensitized with CdS QDs and carbon QDs (CQDs).[126] The ZnO nanorods on ITO glass were hydrothermally synthesized followed by calcination (500 °C) in air and pure ambient H_2 atmospheric pressure at 400 °C. The extension of absorbance within the visible and IR region was made possible following the sensitization of the H:ZnO surface with CdS and CQDs. The optimized H:ZnO/CdS/CQDs displayed a better photocurrent of ~12.82 mA cm^{-2} at 0 V under solar light irradiation. In addition, a novel CdS-intercalated zirconium titanium phosphate (CdS–ZTP) has been prepared by Parida *et al.*, to extend the light absorption toward the visible spectrum while meanwhile inhibiting the fast recombination of charges.[127] Besides, they also found that the surface area of CdS–ZTP material gradually increased with an increased amount of CdS (up to 15 wt%), which is essentially an indirect pillaring effect created by CdS NPs. Pillaring is an important phenomenon that is employed to cross-link the inorganic zirconium-layers and includes materials such as PO_3Zr and ZTP, *etc.* This concept was first described by Dines *et al.*[128], who used rigid aryl groups to cross-link the PO_3Zr layers. Intercalation of pillared materials leads to increases in the porosity and surface area of the layered material, which ultimately have an effect on the catalytic activity.

Plasmonic electron generation

In conductive nanocrystals, localized surface plasmon resonance (LSPR) is often used to boost the absorption capacities of the photocatalysts. Plasmonic materials are employed to enhance the photoresponse of materials in the visible or NIR region. Importantly, the LSPR generally takes place at a higher wavelengths and where there is a coupling between the plasmonic material and the photocatalyst. Jiang *et al.* reported two important effects of the LSPR: (i) the absorption of light and (ii) the hot electron phenomenon (Fig. 3b).[129]

There is a strong electromagnetic field localized around a plasmonic material when excited. The SC absorption overlaps with the created plasmon resonance of the plasmonic material and is subjected to a strong field, so the generation of electrons is greatly increased. This feature is termed the "plasmonic enhancement of light absorption effect". Another effect of (LSPR) is the "hot electron effect" (plasmonic sensitization effect), which refers to the relocation of electrons at the interface between the SC and plasmonic materials.

Duan *et al.* have introduced the concept of multilayer nanoshell plasmonic photocatalysis for photocatalytic production of

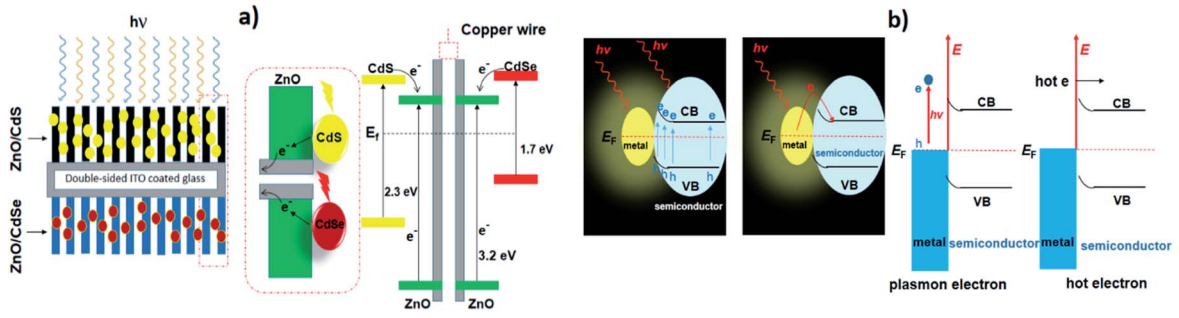

Fig. 3 (a) The architecture and the energy diagram of the double-sided CdS–ZnO–ZnO–CdSe nanohybrids. The mid dashed box represents the CdS–ZnO and CdSe–ZnO interfaces. Reproduced with permission from ref. 125, (b) schematic representation of plasmon-enhanced chemical reactions enhancement of light absorption and hot-electron effect. Reproduced with permission from ref. 129.

H_2 by water splitting.[130] The optical parameters of the Ag/SiO_2/CdS material were investigated and the researchers confirmed that the light absorption ability of this hybrid was markedly enhanced *via* LSPR. By amending the intermediate layers, the resonance wavelength was tuned so that one of the thinner intermediate layers led to a redshift. In another study, hot-electron instillation onto the CdS rod employing optically excited plasmons in the Au tip led to ~2.75% quantum yield. The possibility of further optimization by directing the sizes and morphology of the plasmonic and excitonic domains may lead to a well-designed photocatalyst that can absorb in the broader range of the solar spectrum.[131] Several mechanisms have been proposed to explain the overall chemistry involved and among the many plasmonic materials, the noble metals Ag and Au are the most popular. To prevent the direct transfer of electrons from CdS to the plasmonic material, Torimoto *et al.*[132] introduced SiO_2 around the Au metal. Shell CdS NPs immobilized on Au metal coated with SiO_2 particles were designed; the latter served as an insulator to avoid the direct injection of electrons to Au particles from the CB of CdS (Fig. 4). The activity in this regard is dependent on the relocation of electrons from CdS to Au, because of the locally generated electric field, created by the photoexcitation of the LSPR peak of the Au particles.

The distance between Au and CdS materials greatly depends on the size of the Au particle, *i.e.* larger particle sizes lead to improved photocatalytic activity.

Based on the LSPR mechanism, Au has been used to modify CdS to enhance its photocatalytic performance.[133] Li *et al.* have developed a sandwich CdS–Au–TiO_2 heterostructure as a photoanode for H_2 generation from water.[134] The Au NPs which fit in between TiO_2 and CdS-QD play two roles: (i) as an electron transmitter, which assists the electron transportation between TiO_2 and CdS; and (ii) as a plasmonic photosensitizer to extend the absorption spectrum to longer wavelengths. A photocurrent of 4.07 mA cm^{-2} at 0 V (*vs.* Ag/AgCl) in the presence of Au was achieved with a solar-to-chemical energy conversion efficiency of 2.8%. The incorporation of Au NPs reduces the trap-state, promotes the charge-transfer, hampers the charge recombination, and compensates the undesirable effect of surface trap states. The plasmonic technique is found to provide a swift transfer of the plasmonic hot carriers, a phenomenon that encourages the relocation of electrons at the interface between the SC and the plasmonic material. The interfacial Schottky barrier height (an energy barrier for an electron at SC–metal junction) controls not only the back-transfer of electrons but also controls the plasmonic hot-electron transfer. To gain insight into mechanistic aspects of Au-doped CdS for H_2 generation, the CdS–Au plasmon exciton interaction (as explained above) has been studied by transient absorption spectroscopy. The excitation of the optical plasmons in the Au tip jumps to a hot-electron containing CdS. Impressively, by employing these methodologies, an excellent QE of ~2.75% has been achieved.[131]

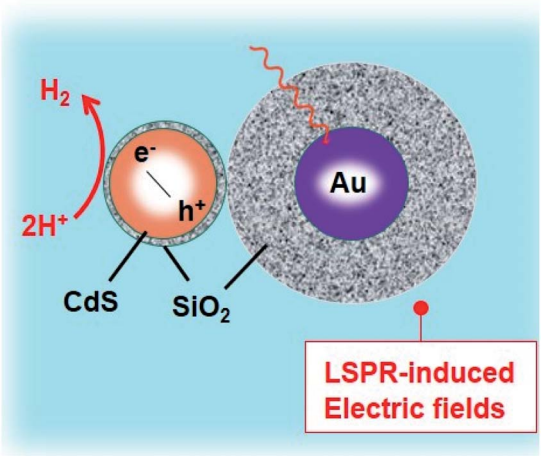

Fig. 4 LSPR-induced electric field immobilized on Au core-SiO_2. Reproduced with permission from ref. 132.

Charge life times in CdS

The transportation of photogenerated charges to the target site is essential in photocatalysis. Most of these pairs are lost through recombination.[135] To address this problem, the concentration of defects in a catalyst material can be reduced by shortening the distance between the charges (electron/hole) and the target site on the surface of the photocatalyst. For this purpose, morphology engineering, structural engineering, cocatalyst strategies, the use of heterojunctions and Z-schemes for CdS as a model photocatalyst, have been investigated.

Morphology and structural engineering for induced charge separation

The process of introducing anisotropy into a photocatalytic system is referred to as morphology engineering, which can help in the survival of electrons. Various SC nanostructures have been produced with different shapes, sizes, crystallinities, and morphologies. In addition, several methods have been reported for the nanoscale formation of CdS, such as solvothermal, chemical vapor deposition (CVD), and thermal decomposition processes.[136–139] All these approaches aim at controlling the morphology, crystallinity, and size of the CdS nanocrystals in the form of nanorods, cubes, tetrapods, hexagons, and pyramids. For example, CdS nanoribbons have been prepared *via* a vapour transport procedure,[140] while CdS nanowires were obtained using a silica template[141] and dendritic CdS nanostructures were hydrothermally synthesized.[142] It is crucial to control the size and morphology of the materials, as the resulting physiochemical properties are strongly affected. However, it is difficult to obtain a nanoscale CdS single crystal that possesses a high dispersibility, even by using surfactants to decrease agglomeration. Consequently, CdS single crystals have been obtained *via* several processes involving reverse micelles, organic solvents, or under harsh conditions.[143,144] The preparation of such crystalline materials with good dispersibility in aqueous phases leads to the possibility of hydrophobic–hydrophilic interactions. This approach promotes charge separation and enhances the rate of photocatalytic reactions.

As mentioned earlier, there are two types of recombination that limit the photocatalytic activity of CdS. One occurs in the bulk, while the other happens on the surface of the photocatalyst. Recombination in the bulk has been overcome by fabricating various CdS nanostructures to facilitate the channelling of electrons. Recently, Kundu *et al.* have prepared different morphologies of CdS and employed them as photoanodes for photoelectrochemical H_2 generation.[3] They envisaged that the enhanced activity of the CdS microspheres mostly depends on the shape rather than the effective surface area. Further analysis of these morphologies revealed that the microspheres were mainly composed of one-dimensional (1-D) structures, such as nanoneedles and nanorods with small surface areas of 19.0 $m^2\ g^{-1}$ and 7.5 $m^2\ g^{-1}$, respectively. Moreover, it was claimed that nanorods and nanoneedles exhibit a better activity than do nanobelts and nanowires despite their large surface areas (32.8 $m^2\ g^{-1}$ and 83.9 $m^2\ g^{-1}$, respectively). The significantly enhanced activity of all these materials has been attributed to superior charge transport and reduced charge recombination. Besides, they also demonstrated that both surface area and shape contribute equally to the catalytic activity of CdS nanostructures. They fabricated different CdS crystal morphologies by a simple hydrothermal method in which they controlled the volume ratio between water and ethylenediamine (en)[3] (Fig. 5A and B). Other factors, such as temperature, precursor ratio, and precursor combinations were also examined. The variation in just the CdS : water ratio (1 : 1, 1 : 3, 3 : 1) led to the formation of different CdS nanostructures, such as nanobelts, nanorods, and nanoplates.

The efficacy of the particle in facilitating charge transport in the crystal may be important. To examine this effect, Pham *et al.* developed a convenient method to produce highly single-crystalline CdS nanocrystals using cetyltrimethylammonium bromide (CTAB, a capping agent) and demonstrated the impact of CTAB on the crystallinity of CdS single crystals to improve the photocatalytic activity of CdS.[145] The interactions between the crystalline facets (001) and the tailored surfactants (CTAB) are the cause of this uniform single-crystalline growth of CdS nanocrystals along the (100) direction. CTAB has been used in the preparation of other metal sulfides,[146,147] but there have only been a few reports regarding CdS. The crystal growth of CdS can be well controlled in the presence of a passive agent such as a surfactant. Moreover, by changing the precursor (sulfur source) and solvent ratio, CdS microspheres with different blocks, such as nano-wires (SNW), nanorods (SNR), nanobelts (SNB) and nano-needles (SNN), were obtained.[145] These morphologies were further tested quantitatively as photocatalysts for photocatalytic water splitting (Fig. 5C).

Among the nanostructures obtained, the catalytic activity of CdS SNR and SNN were found to be better than those of SNW and SNB since the recombination rate in SNW/SNB was more than SNR and SNN due to a large number of defect centres in the former. The main advantage of this work over other studies was the lower temperature (150 °C) and a shorter time (8 h). Similar studies were conducted to fabricate spherical CdS nanostructures using a water/en mixed solvent at ≥180 °C for 24 h *via* hydrothermal route.[148,149]

Guo *et al.* have demonstrated that the efficiency in the photocatalytic behavior of nanocrystalline materials depends not only on size, surface chemistry, and composition but also on the morphology.[150] They successfully controlled the morphology of 3-D assemblies of CdS nanocrystals using an additive-free solvothermal method. Further work revealed that the pH of the reaction media and the cadmium sources also have a marked effect on the morphology of the resulting CdS crystals. All these approaches demonstrate that the catalyst morphology is pivotal in obtaining effective charge separation. Bao *et al.* have produced hollow nanorods and porous nanosheets *via* a two-step aqueous route involving the precipitation of a $Cd(OH)_2$ intermediate followed by ion exchange (S^{2-}/OH^-).[151] A very high H_2 evolution rate of 4.1 $mmol^{-1}$ was observed under 420 nm irradiation, corresponding to the highest QE (60.34%) so far reported for CdS when loaded with 3–5 nm Pt nanocrystals. Another morphology-controlled synthesis of CdS photocatalysts has been reported by Wang *et al.* who fabricated novel 3-dimensional (3-D) flower-like

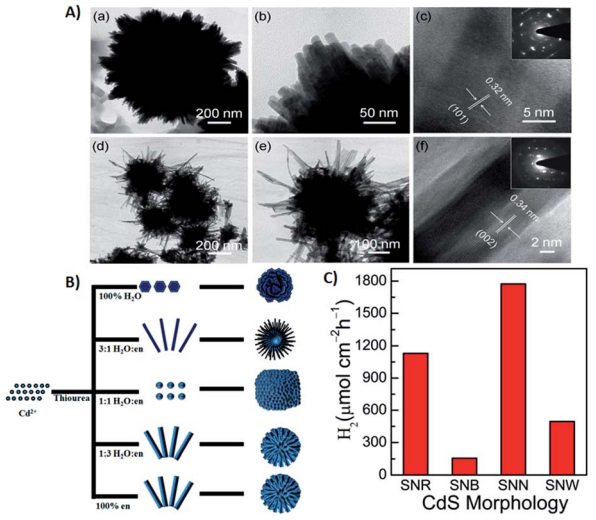

Fig. 5 (A) (a and b) TEM images of CdS nanorods obtained with 3 : 1 water : en solvent; (c) HRTEM and inset SAED pattern; (d and e) TEM images of CdS nanobelts obtained with 1 : 3 water : en solvent; (f) HRTEM and inset SAED pattern, (B) schematic diagram of synthesized CdS morphologies in different solvent media. Reprinted with permission from ref. 3, (C) photoelectrochemical H_2 generation rate of different CdS morphologies under visible light irradiation. Reprinted with permission from ref. 145.

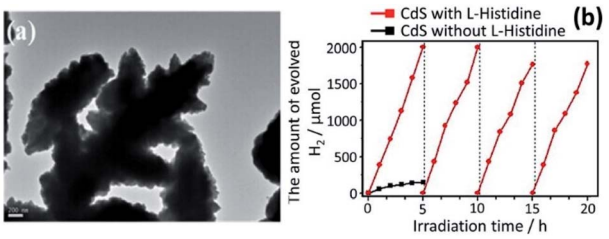

Fig. 6 (a) Morphological analysis of flower-like CdS through TEM analysis, and (b) photogeneration of H_2 on flower-like CdS with and without L-histidine. Reprinted with permission from ref. 152.

materials by a template-free solvothermal technique using $Cd(NO_3)_2 \cdot 4H_2O$ and thiourea and an L-histidine (chelating agent).[152] The comparative study of both pure and 3-D "flower-like" CdS was investigated for photocatalytic water splitting (Fig. 6a). The flower-like CdS exhibited better photocatalytic activity (13 times of CdS). For the CdS with L-histidine, the rate of H_2 was increased up to 376.7 μmol h^{-1} using an aqueous medium comprising 0.5 M of Na_2S and Na_2SO_3 while for the CdS without L-histidine, the rate was only 29.2 μmol h^{-1} (Fig. 6b). Similarly, the photocurrent response of the flower-like CdS material was better (*i.e.* double) than that of pure CdS. This enhancement in performance was ascribed to the effective charge separation and to the high surface area of CdS/L-histidine. A growth mechanism was proposed for flower-like CdS. The Cd^{2+} ions in the solution were captured by the imidazole ring of L-histidine, thus avoiding the agglomeration of CdS NPs.

Novel multi-armed CdS nanorods were synthesized by Yu *et al.*[153] by using a solvothermal method employing dodecylamine as a solvent. The nanorods fabricated by this method displayed prolonged activity in the presence of Pt and lactic acid. The rate of H_2 production, 1.21 $mmol^{-1}$ over 12 h, was about 3.2 times greater than with simple CdS NPs. Moreover, with a substantially lower content of Pt (0.23 wt%), a QE of 51% was achieved. The high activity was ascribed to the positive synergistic effect created by several aspects, such as an adaptation of the hexagonal phase, nanorod morphology, good crystallization, and greater pore volume. Additionally, the hexagonal CdS nanorods revealed good photostability and no photocorrosion after recycling. Lamellar and granular CdS nanostructures of different shapes, *e.g.* nanorods, branches, and cauliflowers, have been synthesized *via* a hydrothermal route using deionized water (as a coordination agent) and en as a template.[154] Interestingly, the morphology of the CdS NPs was dictated by the concentration of en and both $Cd(NO_3)_2 \cdot 4H_2O$ and thiourea. The nucleation of CdS during the decomposition of Cd–en complex is the key step for determining the shape, which in turn depends on the en concentration. A 30% en content leads to the formation of branched CdS NPs, while a 70% en content yields the cauliflower shaped particles. In the presence of pure en, however, hexagonal CdS nanorods were obtained. The morphologies were tested for photocatalytic H_2 production (2577 μmol produced by 0.05 g CdS nanorods over a 4 h period). The rate of H_2 production for the CdS nanorods was approximately 43 times faster than agglomerated lamellar and granular CdS which is attributed to the controlled and effective charge separation in the nanorods, due to channelling of electrons.

Apart from morphology tuning for inducing charge survival, the strategy of directional charge separation has also been applied at a molecular level between structurally engineered CdS and photoelectron conducting species. This approach affords another type of self-modification for electron survival. The electric field generated between CdS and the conducting species is the basis of this separation. Liao *et al.* have described how a conducting head-to-tail (HT) poly-(3-hexylthiophene-2,5-diyl) (P3HT) polymer can be used to control the morphological aspect of CdS nanocrystals as well as the photoelectron conduction for effectual charge separation.[155] All these reports reveal that directional charge separation can be obtained by structural tuning.

Cocatalysts loaded CdS for charge separation

The separation and collection of photogenerated charges and their transportation to the reaction sites greatly reduce the chances of recombination and so charge carriers are protected. The function of a cocatalyst is to catalyse the photocatalytic reaction rather than triggering the HER under light irradiation. Moreover, the cocatalyst acts as a sink for collecting the photogenerated charges as well as serving as the source of active sites for HER.[77] It is generally believed that H_2 activity in the presence of cocatalysts can be increased by at least one order of magnitude. Noble metal-loaded-CdS, such as Pt/CdS,[156] Pd/CdS,[157] Au/CdS,[158] Rh/CdS[159] and Ag/CdS,[121] are promising photocatalysts for water splitting. And if we take Pt as an example, the mechanism of H_2 generation from water splitting using CdS as a photocatalyst is illustrated in Fig. 7.[160] Under solar light irradiation, the separation of photogenerated charges occurs at the interphase between Pt and CdS. The lower Fermi level of Pt compared to CdS and the higher work function is the key driver behind the effective charge separation. Electrons can be relayed easily from the CB level of CdS to the Fermi level of Pt.

This transfer of electrons creates an electron enrichment (−ve) at Pt and an electron deficiency (+ve) at CdS. The relay of electron and holes away from each other occurs due to the drift current, the force opposing the transfer of electrons.

Ultimately, a dynamic balance is reached, whereby the current resulting from the different electronic levels (e− flow from CdS to Pt) is the same as the drift current (e− flow from Pt to CdS).

Noble metals loaded CdS photocatalysts. Both the surrounding medium and the morphology of metal co-catalyst have profound effects on the resulting photocatalytic activity. To check the influence of the medium on the photoreduction of Pt into CdS, Wang *et al.* have studied the effect of pH during the photoreduction of Pt.[161] In basic solution, the Pt/CdS

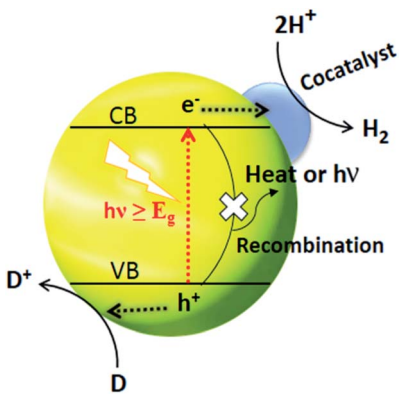

Fig. 7 Cocatalyst triggered photocatalytic process where D and D^+ represent an electron donor and its oxidized form respectively. Reproduced with permission from ref. 160.

photocatalyst generated up to ~1300 μmol h^{-1} of H_2 – much more than in a neutral or acidic solution. Moreover, Pt was photoreduced in basic media showing an excellent activity irrespective of the morphology and crystal structure of CdS. Similarly, the nanocomposite synthesized by Silva *et al.* exhibited high photocatalytic activity (1.0 mmol g^{-1} h^{-1}) with respect to H_2 production from water at pH 14.[162] In contrast, the same system produced only 0.15 mmol g^{-1} h^{-1} (at neutral pH in water/isopropanol media).

Yan *et al.* have prepared Pt–PdS/CdS, a photocatalyst that achieved a QE of up to 93% and produced 8.77 mmol h^{-1} H_2 with the extremely low loading of Pt (0.30%) and PdS (0.13%) as cocatalysts to CdS.[163] Besides, the Pt–PdS/CdS material showed high stability for more than 100 h. Also, Xin and coworkers deposited Pt as a cocatalyst onto CdS *via* coprecipitation and subsequent annealing.[164] The H_2 evolution activity reached a maximum at 450 °C (~300 μmol h^{-1} g^{-1}) and decreased beyond this temperature, which may be due to the incomplete oxidation of H_2PtCl_6 and poor crystallinity of the catalyst. In addition, Yao *et al.* demonstrated the rates of H_2 evolution from photochemically treated Pt/CdS, which were compared with those from untreated Pt/CdS; the H_2 production rates were 4.8 μmol h^{-1} and 644.1 μmol h^{-1}, respectively.[156] Jin *et al.* investigated the effect of reduction ($NaBH_4$ reduction and photoreduction deposition) for Pt deposited onto a CdS photocatalyst.[165] Pt deposition *via* reduction using $NaBH_4$ resulted in a higher photocatalytic activity than when Pt was deposited through the photoreduction process. A significant H_2 evolution rate of 1.49 mmol h^{-1} (QE of 61.7%) was obtained with a minor amount of Pt (0.3%) loaded onto CdS. The reduction method strongly influences the size and distribution of the Pt NPs, which in turn alters the activity of the photocatalyst.

The effects of the morphology of the Pt particles on the activity of the Pt/CdS material has been investigated. In this study, nanocubic and nanospherical Pt particles were prepared and deposited on CdS separately.[166] The H_2 production rate was 52% higher in the case of the Pt nanocubes. Besides, Pt nanocubes (5.7 and 4.0 nm), loaded onto CdS, exhibited 52% and 31% more activity compared to the same size of nano-spherical Pt particles. This feature arises from several factors: first, spherical particles have smaller volumes than the cubic ones, and, therefore, the possibility of aggregation in the case of spherical Pt NPs is higher than with the Pt nanocubes. Second, the atom density of crystal planes of Pt nanocubes for proton adsorption is higher than that of the nanosphere; and third, the contact of CdS crystals with Pt nanocubes is better than that of the Pt nanospheres, which reduces the impedance between CdS and Pt particles and, therefore, prevents energy loss during charge transportation.

Sahu *et al.* have studied the kinetics of H_2 production using alumina as support under visible irradiation; the reaction rate initially increased and then decreased.[167] They observed a negligible induction period upon illumination of the catalyst, which is due to the readsorption of sulfide ions on the Pt/CdS catalyst surface, while the decrease in the rate was attributed to the deactivation of the catalyst by H_2. Zhou *et al.* anchored CdS and Pt NPs in a highly dispersed form in the mesoporous channels of zeolite beta by applying a two-step pore modification strategy.[168] A rate of 3.09 mmol h^{-1} g^{-1} was achieved which could be ascribed to the synergetic catalytic chemistry between Pt and CdS, the interaction between CdS and the zeolite matrix, and the highly dispersive form of the CdS and Pt particles.

Sakamoto *et al.* successfully deposited 1 nm Pt NPs on a CdS nanostructure using a wet-chemical method and reported that Pt deposition shows a higher catalytic activity.[169] To prepare this system, first, Pt ions are accumulated on the S 21 inch surface of CdS, followed by a reduction of oleylamine to form the Pt core. These cores grow gradually as more Pt ions are reduced and accumulate on the Pt NPs. Depending on the amount of oleylamine used, the diameter of the Pt NPs remains approximately 1 nm. Shen *et al.* dispersed Ag_2S in the CdS nanostructure to investigate its activity toward H_2 production in water splitting with the sacrificial reagent Na_2S/Na_2SO_3 being present as a hole trapper.[170] The Ag_2S/CdS material (with Ag_2S 5% by weight) exhibited better photoactivity with an external quantum yield (EQY) of 0.7%. Also, Li *et al.* have studied the hydrothermal transformation of the cubic-phase CdS nanocrystal into its hexagonal form by treatment with Na_3PO_4 at 180 °C for 12 h.[171] They also studied the effects of hydrothermal time, Pt loading, and phosphate concentration on H_2 evolution from aqueous solutions (containing formic acid as a hole scavenger). The phase alteration from the cubic to the hexagonal form was markedly promoted by the phosphate ions. The hexagonal CdS photocatalyst exhibited a higher rate of H_2 activity compared to the cubic phase. Moreover, Pt (0.025 wt%) loaded CdS showed excellent activity with an apparent quantum yield of 21.4%.

Large-scale CdS nanorods, nanostrips, and plates have been synthesized *via* solvothermal techniques using a cadmium oxalate precursor and $(NH_4)_2S$ as a sulfiding agent.[172] The aspect ratio of the nanorod lengths varied from 3 to 30 nm. Comparative photocatalytic activity studies were conducted on a CdS, calcined CdS, and noble-metal loaded CdS nanorods. The nanorod loaded with Pt proved to be highly effective compared to bulk CdS. The 0.2% Pt loaded sample evolved 26 mL of H_2 in 6 h, while the activity of bare CdS was less efficient. It was further noted that beyond the optimum amount of Pt deposition, the partial blockage of the CdS surface by metallic Pt NPs occurs, which shields it from the adsorbing photons.

Wang *et al.* have prepared wool-supported Pd co-catalysts, which were then loaded at an optimal weight percentage (3.0 wt%) onto CdS.[173] A high photocatalytic H_2 production activity rate of 1555 μmol h^{-1} was observed. The better catalytic performance was credited to the recycled co-catalyst, wool–Pd that introduced an oxidised (PdS) and reduced (Pd) cocatalyst. For direct conversion of solar into H_2 energy, Yan *et al.* have developed a photocatalyst composed of Pt–PdS doped CdS with a QE of 93%.[108] The better QE was achieved with very minimal loadings of Pt and PdS onto CdS (0.13 wt% of PdS and 0.30 wt% of Pt). In combination with a noble metal, transition metal oxides proved to be highly effective in HER. Yao *et al.* have used Pd and Cr_2O_3 nanocomposites as cocatalysts and loaded them onto a CdS photocatalyst.[174] The HER was higher for Pd–Cr_2O_3/CdS (2.27 mL min^{-1}) than for the plain Pd metal (1.64 mL min^{-1}) loaded catalyst at room temperature. The shape-

dependent effect of Pd nanostructures on the photoactivity of CdS has been investigated by Luo *et al.*[175] Nano-cubes (NCs) and nano-octahedra (NOTs) of Pd nanostructures were prepared by a morphology-controlled method and were deposited onto commercial CdS, and the photocatalytic activity of the Pd/CdS was determined in the presence of an ammonium sulfite (sacrificial reagent). The NCs were enclosed by six {100} facets, while the NOTs were enclosed by eight {111} planes. The Pd-NCs doped CdS (Pd-NCs/CdS) exhibited higher activity (1.38 times than that of Pd-NOTs/CdS) due to the Pd {100} crystal facets of the Pd NCs and the higher electrochemical active surface area (ECSA).

Many studies have explored the synthesis of PdS and its use as a cocatalyst on CdS, *e.g.*, Chen *et al.* have developed efficient supports for overall water splitting (in the presence of PdS and Na_2S/Na_2SO_3 as a hole scavenger).[176] The 1 wt% loading of PdS onto CdS, prepared by an *in situ* coprecipitation method, exhibited better photoactivity and stability than prepared by hydrothermal methods. Bi-metal cocatalyst incorporation on CdS, *e.g.*, Pt–Pd NPs, at an appropriate loading has been studied by Li and coworkers.[177] A notable H_2 evolution rate of 25.28 mmol h^{-1} g^{-1} (Pt–Pd/CdS) was recorded under visible irradiation (300 W Xe light, $\lambda > 420$ nm), which was 2.4 and 3.8 times higher than that obtained for Pt/CdS and Pd/CdS respectively. The improved catalytic activity of Pt–Pd/CdS was ascribed to the effective suppression of charge recombination.

Owing to the unique optical, magnetic, electronic and catalytic properties, Au NPs have appeared as a new class of material.[178] Recently, Zhao *et al.* found that combining CdS QDs and Au NPs under certain conditions results in the transfer of electrons and energy between particles (Au NPs and CdS QDs).[179] The CdS-QDs/Au-NPs nanohybrids apparently promote charge separation and enhanced catalytic activity. Similarly, Xing *et al.* have prepared the novel nanohybrid, CdS-QDs/Au-NPs@POM, by a self-assembly scheme.[180] The POM ($H_3PW_{12}O_{40}$) material was employed as an encapsulating, reducing, and bridging molecule in the hybrid system. Interestingly, the resulting nanohybrid exhibited very high photocatalytic H_2 evolution in water splitting.

Also, Shemesh *et al.* have prepared two novel nanohybrid materials containing CdS as the photocatalyst and Pd compounds (PdO and Pd_4S) as cocatalysts.[181] The CdS–PdO material was prepared by an aqueous phase hydrolysis method and CdS–Pd_4S was designed *via* a high-temperature treatment (using a reduction method) followed by cation-substitution. The desired CdS nanorods of varying diameter were prepared and injected into a solution of Pd(II) acetylacetonate. The new nanohybrids were tested for the photoreduction of water. The nanohybrid maintained the CdS morphology, but some sites clearly showed more contrast at the tips of the CdS nanorods (Fig. 8a).

Palladium oxide (PdO), was more catalytically active than other small NPs, such as gold. Nano-SCs may elevate the CB level due to quantum confinement effects to assist in the reduction process and make it more thermodynamically favorable (0.03% yields). Moreover, the small NPs may exhibit

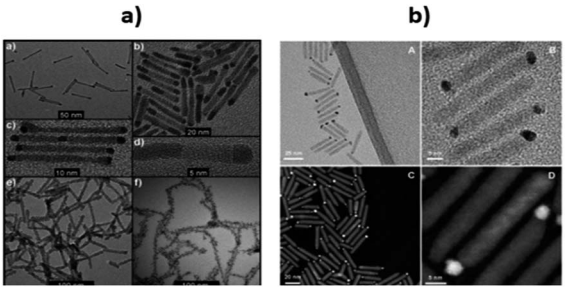

Fig. 8 (a) (a) Pd_4S growth on CdS nanorods; (b) size distribution of CdS nanorods decorated by Pd_4S; (c) close-up of the sample shown in (a); (d) HRTEM of a single CdS–Pd_4S nanohybrid of the sample shown in (b); (e) PdO growth on CdS nanorods; (f) CdS nanorods decorated with large dots of PdO. Reprinted with permission from ref. 181. (b) TEM (A and B) and HAADF (C and D) images of CdSe@CdS nanorod with Au–Pt bimetallic. Reprinted with permission from ref. 182

a greater number of reactive step-edge sites and therefore, boost the photocatalytic activity.

Further improvement in the productivity of photocatalytic water splitting was accomplished by Kalisman *et al.*, who used the bimetal Au–Pt as a cocatalyst[182] (Fig. 8b). They prepared CdSe@CdS nanorods tipped with Au decorated Pt. Simply, by varying and adjusting the composition and shape-engineering of Au–Pt, they achieved an impressive H_2 production rate compared to pure Pt. The strategy of coupling Au with Pt, grown on CdSe@CdS nanorods leads to the formation of a promising single catalytic reduction site.

The synthesis of colloidal tetrashaped CdS nanocrystals *via* a low-temperature phosphine-free method and in the presence of sodium diethylcarbamodithioate or thioacetamide has been undertaken.[183] Using different sulfur sources, the growth of CdS particles was controlled to tune the arm length and diameter of a CdS tetrapod. Then, Au incorporation onto CdS to form the Au/CdS nanohybrid was demonstrated towards HER. In the presence of Au, the tetrapod CdS nanohybrid displayed excellent photoactivity.

To study the role of the oxidation catalyst, Tseng *et al.* have studied the charge-transfer relations between the photoexcited CdS nanorods and the water oxidation catalyst resulting from $[Ru(bpy)(tpy)Cl]^+$.[184] The photogenerated hole in the VB of CdS oxidized Ru^{2+} to Ru^{3+} (100 ps) followed by a reduction of Ru^{3+} back to Ru^{2+} (10–100 ns). The advantage of this slow dynamic electron-transfer is that it may provide an opportunity for holes to oxidize water molecules.

Non-noble metals loaded CdS photocatalysts. Due to the high cost of noble metals, it is very difficult to use them in commercial H_2 technology. There is, therefore, a major incentive to develop low-cost cocatalyst materials, such as low-cost transition metals,[185–189] MoS_2,[190] tungsten carbides (WC),[191] and graphene[192–194] deposited on CdS. These materials have good activity for H_2 generation, and, in some cases, they even surpass the noble metal-doped CdS systems. The surface modification involves the use of different capping agents, which not only prevent the agglomeration of NPs but also control their size by modifying the kinetics of their growth. Additionally,

surface modification creates quantization in the NPs, which in fact makes them appropriate materials for photocatalytic water splitting. Lee *et al.* have prepared CdS NPs *via* an *in situ* method on the porous titanium oxide films and then used them in fabricating photoelectrodes.[118]

Non-noble metals doped CdS photocatalysts, such as Ni–CdS QDs, have been reported to be one of the most robust materials for the artificial photocatalytic release of H_2 from water. CdS QDs, capped with 3-mercaptopropionic acid, can be reacted *in situ* with Ni salts for the synthesis of Ni hybrid CdS QDs. As compared to CdTe and CdSe QDs, surface-modified CdS QDs have a greater affinity for Ni^{2+} and very high efficiency for H_2 production.

Liu and coworkers have managed to dope CdS with Mn^{2+} and found that the crystal phase, band gap, and morphology of CdS remain intact.[195] A doping content of 0.5 wt% doubled the H_2 production rate (300 μmol h^{-1} $g_{cat}{}^{-1}$) compared to that for bare CdS. The Mn^{2+} ions serve as shallow trapping sites for electron–hole pair separation. Moreover, the apparent quantum yield (AQY) value reached 5% using 0.5 wt% doping indicating that the photoactivity of CdS can be enhanced by Mn^{2+} doping. As discussed in the previous section, the noble metals (Pt, Pd, Rh) are very effective active sites for proton reduction (as they act as electrons traps).[196,197] Similarly, a non-noble metal, such as Ni and its compounds such as NiS, NiO, $Ni(OH)_2$, and Ni@C, can play the same role as a cocatalyst in the decomposition of water.

To use Ni and Ni compounds as cocatalysts, researchers managed to synthesize successfully various combinations of photocatalysts, such as Ni/CdS, NiS/CdS, $Ni(OH)_2$/CdS, Ni@C/CdS, in efforts to improve the efficiency of the CdS SC.[185–189] These modifications have several advantages with respect to release H_2 from water, as well as providing an economically cheap material for the cocatalyst. In general, the high activity of a NiS/CdS photocatalyst was attributable to the construction of a p–n junction between the NiS and CdS interface, which hampered the recombination of the charge carriers thereby enhancing the H_2 production rate. The activity of $Ni(OH)_2$/CdS was improved significantly, up to a factor of 136 compared to bare CdS (using Na_2SO_3 and Na_2S aqueous solutions).[185] The $Ni(OH)_2$ loaded CdS-nanorods composite was synthesized using a precipitation method. A special focus was given to the influence of the $Ni(OH)_2$ species on the photoactivity of CdS using a triethanolamine aqueous solution. The 23 mol% optimized $Ni(OH)_2$ loaded CdS generated an H_2 production rate of 5085 μmol h^{-1} g^{-1} with 28% QE at 420 nm, exceeding by a factor of 145 and 1.3 compared to pure CdS and 1 wt% loaded Pt CdS nanorods respectively. The improved activity was credited to the suitable reduction potential of Ni^{2+}/Ni^0 ($Ni^{2+} + 2e^- = Ni^0$, $E^0 = -0.23$ V), which was higher than the CB potential of CdS (−0.7 V) and is less than the reduction potential of H^+/H_2 ($2H^+ + 2e^- = H_2$, $E^0 = 0.0$ V). In addition, the role of Ni^0 is to suppress charge recombination when acting as a reduction co-catalyst in water splitting; Ni^0 can easily channel the transfer of electrons and accelerate the rate of H_2 generation.

Simon *et al.* have employed hydroxyl anion/radicals as redox mediators to transport holes from Ni/CdS to the scavenger.[78] A rate of 63 mmol h^{-1} g^{-1} and an apparent QE of 53% were achieved under 447 nm laser irradiation. The high activity was ascribed to the fast-hole channelling effect that confers long-term photostability on CdS and thus improves overall water splitting. Peng *et al.* have prepared Ni@C/CdS and tested it as a photocatalyst (using Na_2SO_3 and Na_2S as a hole scavenger) in aqueous solution for the production of H_2 from water.[198] A rate of 3.328 mmol h^{-1} g^{-1} was observed using a 300 W Xe-lamp ($I >$ 420 nm). The improved performance was attributed to the deposition of metallic Ni on the CdS surface, which was supported by graphite-like carbon acting as an electron acceptor.

Li *et al.* have synthesized graphene nanosheets decked with CdS clusters for use as a visible responsive candidate for highly efficient H_2 production.[199] The graphene/CdS nanocomposite had an excellent H_2 release rate of 1.12 mmol h^{-1}, *i.e.*, 4.87 times greater than that for pure CdS NPs. Moreover, for a 1.0 wt% graphene and 0.5% Pt content, the QE obtained at 420 nm was 22.5%. The improved activity was ascribed to the electron collector ability of graphene and the channelling of these electrons, thus extending the lifespan of the charge carriers. The electrons were promoted from the VB of CdS to the CB and then were channelled in three ways. First, the electrons were trapped by the deposited Pt, followed by the carbon atoms in the graphene nanosheets and then by the metallic Pt on the graphene nanosheets. The adsorbed H^+ ions were reduced by these electrons to generate H_2 gas. As previously mentioned, the CB of CdS is more negative than the reduction potential of H^+/H_2; however, using bare CdS, the H_2 activity was negligible due to the rapid recombination of the photogenerated electron–hole pairs. In the presence of graphene, the electron collection and transfer are enhanced, which suppresses the charge recombination process. Importantly, in the presence of graphene, the proton reduction reaction not only occurs on the surface of the catalyst, but also over the graphene nanosheets themselves[199] (Fig. 9). In the case of N-graphene/CdS, the electrons are transferred preferentially from CdS to the N-doped graphene.[192] The recombination of the photogenerated charges, in this case, was effectively suppressed, which enhanced the photocatalytic activity. The activity order (N-graphene/CdS > graphene/CdS > GO/CdS > CdS) in this regard showed that N-graphene/CdS has better stability for H_2 production over a period of more than

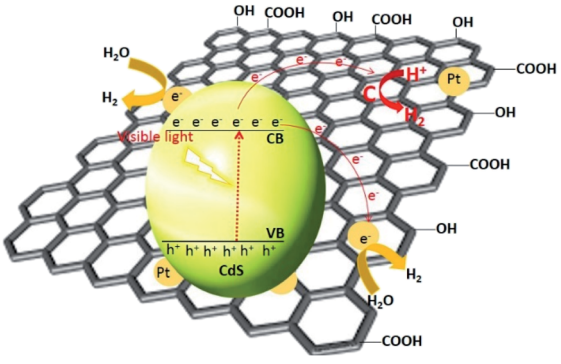

Fig. 9 Proposed mechanism for the charge separation and transfer in the graphene–CdS under visible light irradiations. Reproduced with permission from ref. 199.

30 h, revealing that N-graphene, acting as a cocatalyst, can inhibit CdS from photocorrosion. Thus, N-graphene is a promising cocatalyst for use in developing a high-performance CdS photocatalyst for H_2 generation.

CdS-based heterojunctions

A heterojunction is simply a hybrid photocatalytic system constructed from two different SCs. The built-in electric field is created at the interface of two SCs owing to the difference in Fermi levels. There are three types of heterojunctions that are classified as the band alignment straddling gap (type-I), the staggering gap (type-II), and the broken gap (type-III)[200] (Fig. 10).

In type-I heterojunctions, the VB and CB levels of the narrower band gap are enclosed in those of the larger one. Also, in a type-I heterojunction, charges are pushed towards a narrower band-gap SC, where they easily recombine. In type-II heterojunctions, CB and VB levels are staggered between two SCs, thus creating an accumulation of opposite charges at the respective sites and so preventing recombination of the charges. Type-II heterojunctions, which are considered to be more effective, comprise two classes. One class is formed by a single SC having two phases, *i.e.*, a heterophase, such as the heterojunction formed with the TiO_2(B)–anatase heterophase. The second is formed by two different SCs, and has been demonstrated to be highly efficient, *e.g.*, the CdS/CdSe[201] and CdS/g-C_3N_4,[202] CdS/TiO_2 (ref. 203) heterojunctions. In type-III heterojunctions, charge suppression is hard to achieve as the CB level of one SC lies just below that of the other SC, where charge recombination is dominant. These types of heterojunctions are rarely applied in photocatalysis.

The SCs $BiVO_4$,[204] Ta_3N_5 (ref. 205) and Ag_3PO_4 (ref. 206) are known for their role in O_2 evolution, while the CdS photocatalyst is especially efficient for H_2 evolution;[47] however, as discussed above, some associated issues hamper its activity. Hence, CdS-based heterojunctions have been developed to overcome the recombination phenomenon, poor stability, and particles agglomeration. Notable examples include the formation of a Pt–PdS/CdS heterojunction with a very stable QE of 93% for H_2 generation when it contains Ag_2S/CdS.[170] The holes in Ag_2S oxidize sulfite ions, which are the hole scavengers. Besides, the junction formed between CdS and TiO_2 nanotubes results in improved photocatalytic performance because of the ease of electron transportation from the CB of CdS to the CB of TiO_2.[207] Moreover, in the presence of a reduction metal cocatalyst, such as Pt, the heterojunction system displays the same electron-transfer phenomenon in a more controlled way.[208]

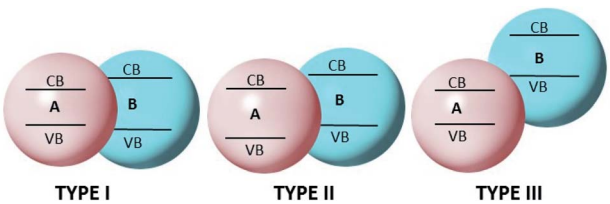

Fig. 10 Band alignment in type I, II, and III heterojunctions.

A very high current density (12 mA cm^{-2} at 0 V *vs.* Ag/AgCl) has been recorded for CdS/ZnO/ZnO/CdSe nanowire arrays in PEC water splitting.[125] In this heterojunction system, the position of the Fermi levels of all species (CdS, CdSe and ZnO) are so aligned that the CB of CdSe and CdS are close enough to permit electrons (created in CdSe) to delocalize and redirect to ZnO *via* the CdS layer. In a report published by Moriya *et al.*, a thin coating of CdS on Pt/$CuGaSe_2$ – an active p–n heterojunction – achieved not only a 10 days long term performance for photoelectrochemical (PEC) water splitting, but also had 6 times greater photocurrent response than did Pt/$CuGaSe_2$ (ref. 209) (Fig. 11). The markedly enhanced activity was ascribed to the facile charge suppression between these two materials because of the p–n junction created and the optimum increase in the thickness of the depleted region at the interphase of solid-electrolyte. Moreover, the different position of the VB offset between the two materials (0.98 V) was the reason behind the electron diffusion into CdS from $CuGaSe_2$ (CB –0.8 V and VB +0.9 V *vs.* NHE). More details on different CdS based heterojunctions are discussed in the following sub-sections.

CdS/MoS_2 based heterojunction. Zong and coworkers have developed a MoS_2/CdS heterojunction, using lactic acid as an electron-donor species to produce H_2, *via* photocatalytic water splitting.[190] The activity of CdS loaded by MoS_2 was notably better than that for Pt/CdS (under the same reaction conditions). To examine the effect of loading, CdS alone only released 15 μmol h^{-1} H_2, while 0.01 wt% loading evolved up to 22 times more. Increasing the doping content up to 0.2 wt%, caused the rate to increase by a factor of 36 compared to bare CdS. Similarly, Xu and Cao discovered strong interactions between MoS_2 and CdS.[210] For loadings of 2.0 wt% of MoS_2 on CdS, the rate was boosted 17-fold (4.06 mmol h^{-1} g^{-1}, H_2 production). A similar approach was undertaken in PEC studies of an MoS_2/CdS photocatalyst for the generation of H_2.[211] The p–n junction between MoS_2 and CdS was successfully established by an electrodeposition method. The new material showed high photocatalytic activity. For a 0.14% MoS_2 sample loaded onto CdS, an impressive photocurrent of 28 mA cm^{-2} was obtained with incident photon-to-current conversion efficiency (IPCE) of 28. Moreover, Liang *et al.* have prepared some MoS_2 QDs/CdS core/shell nanospheres using L-cystine as a sulfur source by a hydrothermal method, which exhibited improved photoactivity compared with pure CdS NPs.[212]

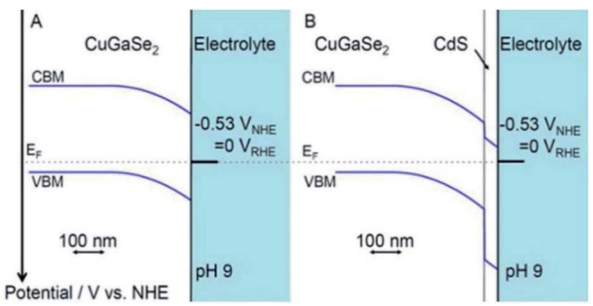

Fig. 11 Band alignment at interfaces for (A) $CuGaSe_2$ and (B) CdS/$CuGaSe_2$ electrodes. Reprinted with permission from ref. 209.

A 2-D hybrid system, consisting of CdS nanosheets and an MoS_2 layer, has been developed *via* a two-step hydrothermal and ultrasonic treatment. The loading of an appreciable amount of MoS_2 onto CdS nanosheets enhanced their photocatalytic activity. Furthermore, the optimized 2-D CdS/MoS_2 (1.0 wt%) achieved a 1.75 mmol h^{-1} g^{-1} rate of H_2 from water containing sulfide and sulfite ions. This rate was greater by a factor of ~2 compared with pure CdS nanosheets. The intimate 2D–2D contact coupling interface in the material promoted and transported charges to the surface sites. To suppress further the recombination process, formic and lactic acids were introduced as sacrificial reagents.[213] Other electron donor species can also be used to enhance the photocatalytic activity of such junctions, such as lactic acid as reported by Zong *et al.*[190]

CdS/ZnS based heterojunction. Metal sulfide-based heterojunctions, especially CdS/ZnS, are well known among CdS-based photocatalysts, which play a key role in the photocatalytic H_2 generation from water. Du and co-workers have proposed two mechanisms for a CdS/ZnS heterojunction[214] *viz.*, (i) a hole-transfer (A) and (ii) an electron-tunnelling (B) mechanism. Several intrinsic defects including zinc vacancies (V_{Zn}) and interstitial sulphur (Is) in the ZnS SC shell can act as sinks for the holes formed in the VB of CdS which, in turn, hinder charge recombination and therefore lead to an enhanced rate of H_2 production. A tentative mechanism for the efficient photoactivity of a CdS/ZnS heterojunction has been suggested, based on the CB/VB of CdS and ZnS.[215,216] Electrons are promoted from the VB of CdS to the CB, thus creating holes in the VB of CdS. These holes move from the CdS Fermi level to the ZnS Fermi level, *i.e.*, there is a transfer between the two SCs.[217] This spatial separation is probably a bottle-neck in the enhanced activity of the CdS/ZnS heterojunction in H_2 generation. Taking into account the ZnS thickness, another mechanism, based on an electron-tunneling pathway, has been proposed for type-1 heterojunction nanohybrids such as CdSe/CdS, CdS/ZnS. Electrons in surface-deep-trap states of CdS have insufficient energy for H_2 evolution and are passivated to make more photogenerated charge carriers with suitable energy for the proton reduction, and the charge carriers especially electrons in the CdS core might well channel through the thin ZnS shell. Moreover, the photogenerated electrons may also go out from the unexposed surface of CdS to the outside surface. As a result, the pathways discussed above are probably responsible for the efficient photoactivity for H_2 production.

Recently, Xie *et al.* have reported a unique charge-transfer phenomenon for CdS–ZnS core–shell particles in photocatalytic H_2 generation (with 792 μmol h^{-1} g^{-1}) *via* water splitting.[218] They found that electrons and holes cannot transfer to the ZnS shell because the CB energy is higher compared to CdS. Also, the VB of ZnS is more positive than is that in CdS, with the acceptor states lying within the band gap of ZnS, thus allowing hole transfer from the VB of ZnS shell to CdS and promoting efficient charge separation. To overcome the problem associated with type-I heterojunctions, Zhuang *et al.* have prepared a multi-node sheath to accomplish adaptation from a type-I to type-II heterojunction.[219] The [ZnS–CdS]–ZnS–[ZnS–CdS]–ZnS-hetero-nanorods alone displayed type-I behaviour. At the ZnS/CdS interface, the charges are close enough to recombine. After introducing Au, the position of CdS bands alters, which facilitates electron transfer to CdS from Au. The electrons are shifted from CdS to ZnS, creating holes in the VB of CdS, thus separating the charges, therefore converting into a type-II example.

CdS/g-C_3N_4 based heterojunction. The heterojunction between CdS and g-C_3N_4, a type-II system, represents well-defined chemistry between the two SCs. The tentative mechanism for such a junction is as follows. Photoelectrons are transferred from the CB of g-C_3N_4 to the CB of the CdS owing to the difference in the band offsets potential. Subsequently, those electrons promoted from the VB of CdS to the CB of CdS and those transferred from g-C_3N_4 to CdS can be captured by the metallic NPs such as Pt, Ni, *etc.*, which act as a reducing site for H^+ to H_2. As the VB of CdS is lower than is that of g-C_3N_4, hence allowing the migration of holes from the VB of CdS to g-C_3N_4, which leads to the suppression of charge recombination and enhancement of the photocatalytic H_2 generation *via* water splitting.

Inorganic-organic CdS@g-C_3N_4 core–shell nanorods have been prepared by a hydrothermal method.[220] These materials displayed excellent stability against light illumination as compared to pure CdS NRs. Besides, a photocurrent density of 1.16 mA cm^{-2} was obtained (2.5 times of pure CdS NRs). Interestingly, more than 85% of the initial photocurrent was maintained for CdS@g-C_3N_4, while for pure CdS NRs it dropped to 20% after 3600 s of continuous illumination. Some studies are reported on the g-C_3N_4/CdS heterojunction, including a systematic calculation of both the energy of the band gap and charge transfer.[221] The contact between CdS (110) and g-C_3N_4 is known as a van der Waals heterojunction. The formation of a standard type-II heterostructure was the result of changed positions of the band edges of g-C_3N_4 and CdS. Moreover, the calculated Bader charge and the charge density difference show that the separation of the charges at the g-C_3N_4/CdS interface was due to the internal generated electric field.[221] These observations provide evidence for the band structures of the hybrid g-C_3N_4/CdS and its photocatalytic efficiency.

CdS/g-C_3N_4 heterojunction nano-cone arrays, constructed on Si (100) substrates, have also been investigated *via* the plasma sputtering reaction deposition (PSRD) and pulsed laser deposition (PLD) techniques.[222] The g-C_3N_4 nano-cone arrays prepared by PSRD were single crystalline in nature with a [001] growth direction, while deposition of CdS NPs shells by the PLD method had a hexagonal wurtzite structure. The bare g-C_3N_4 nano-cones showed an intense distinctive PL peak at 454 nm. While preparing the hybrid with CdS, peak quenching occurred, showing that the chances of charge recombination had been extensively suppressed because of the spatial charge separation in the CdS/g-C_3N_4 heterojunctions. The absorption edges of the CdS/g-C_3N_4 heterojunctions displayed slight red shifts when CdS was deposited onto g-C_3N_4.

Some CdS/g-C_3N_4 nanowires have been produced by changing the contents of g-C_3N_4 using a combined solvothermal and chemisorption synthetic route.[223] These nanowires have been investigated for H_2 production using Na_2S and

Na_2SO_3 ($\lambda \geq 420$ nm). Preferentially, g-C_3N_4 was coated on CdS (after successful spontaneous adsorption), which resulted in an enhanced photocatalytic activity (H_2: 4152 μmol h^{-1}, g-C_3N_4: 2 wt%). Also, the g-C_3N_4 coating improved the photostability of the catalyst for long term photocatalytic activity. This high activity was ascribed to the synergistic effect created between CdS and g-C_3N_4, which suppressed the charge recombination and redirected the holes from CdS towards g-C_3N_4.

Similarly, CdS QDs coupled with g-C_3N_4, were prepared through a chemical impregnation process. The effect of CdS loading (varying dosage of CdS) on the g-C_3N_4 catalytic activity was investigated in methanol/aqueous solution.[224] This positive synergistic coordination between CdS and g-C_3N_4 leads to effective charge separation and enhanced catalytic activity. A 30 wt% CdS content was shown to be the optimum amount, which evolved 17.27 μmol h^{-1} (~9 times of g-C_3N_4). The CdS QDs/g-C_3N_4 nanohybrid had a bathochromic shift and exhibited a robust absorption capability for the visible light.

CdS/TiO_2 based heterojunction. Chaguetmi *et al.* have designed surface-modified CdS QDs impregnated into TiO_2/Ti and reported excellent efficiency for PEC water splitting.[225] CdS–TiO_2 nanocomposite films supported on the conductive sheet of Ti can be prepared using a three-step method. Surface-modified CdS QDs were prepared by a polyol method and were then incorporated into TiO_2/Ti for efficient H_2 production. The increase in the photocurrent was attributed to the impregnation of the surface-modified CdS QDs in TiO_2/Ti leading to a lower rate of excitonic recombination and greater PEC water splitting. The photocurrent has a prominent role in reducing H^+ to H_2 at the Pt wire as cathodic material (Fig. 12a). Similarly, the CdS-based anodic material can also be engineered, as is the case when the SC that has a CB less negative than the CdS CB is coupled. For example, CdS NPs with modified surfaces that have a CB level (0.5 eV) more negative than TiO_2 can be coupled to produce photoanodes, which could be suitable for photo-electrochemical cell application under visible light irradiations.[226]

Corrosion-resistant photoelectrodes for efficient water splitting consist of surface-modified CdS QDs coupled with TiO_2 as the photoanode and CdSe QD coupled with NiO as the photocathode[227] (Fig. 12b).

The QDs in these photoelectrodes were surface passivated with ZnS shells. These photoelectrodes have an efficiency comparable to that of natural photosynthesis (0.17%) and exhibit excellent photostability in visible light. The surface-modified CdS QDs impregnated with TiO_2 represent an efficient photoanode and CdSe modified by NiO acts as a photocathode where the Cd chalcogenide is protected by a ZnS layer. The optimized system exhibited a photo efficiency of 0.17% comparable to that of natural photosynthesis.

Because of their high molar absorptivity, CdS QDs have been used as potential candidates in photo-electrochemistry and photovoltaics. CdS QDs are deposited on TiO_2-NTs for efficient water splitting. However, CdS NPs tend to aggregate on the surface of TiO_2-NTs, which causes a considerable decrease of contact between these two SCs. The aggregation of CdS QDs results in a low absorption of light and a decrease in charge separation and the charge-transfer rate. Surface-modified CdS QDs have a notable degree of dispersion and impregnation with TiO_2-NTs extends exposure to longer wavelengths and promotes the efficient shifting of electrons between CdS QDs and TiO_2-NTs.[228]

Although CdS QDs are potential contenders for water splitting, the rapid rate of electron–hole pair recombination limits their application in water splitting. However, CdS QDs capped with different surface modifying agents show remarkable properties. Stabilizing agents decrease the size of the CdS NP and result in broadening of the band-gap energy, which preserves the potential barrier for free electrons and holes, and lowers their rate of recombination. In surface-modified CdS QDs, free electrons are readily available in the CB, which is used for photoelectrochemical reduction of H^+ to H_2. CdS QDs have size-tunable band gaps (3.5 to 2.2 eV). These surface-modified CdS QDs can transfer electrons from the CB level of wide-band gap SCs, thus improving the efficiency of energy conversion and providing new opportunities for harvesting energy.

CdS-sensitized TiO_2 NPs have been proposed as efficient materials for photo-electrochemical water splitting under

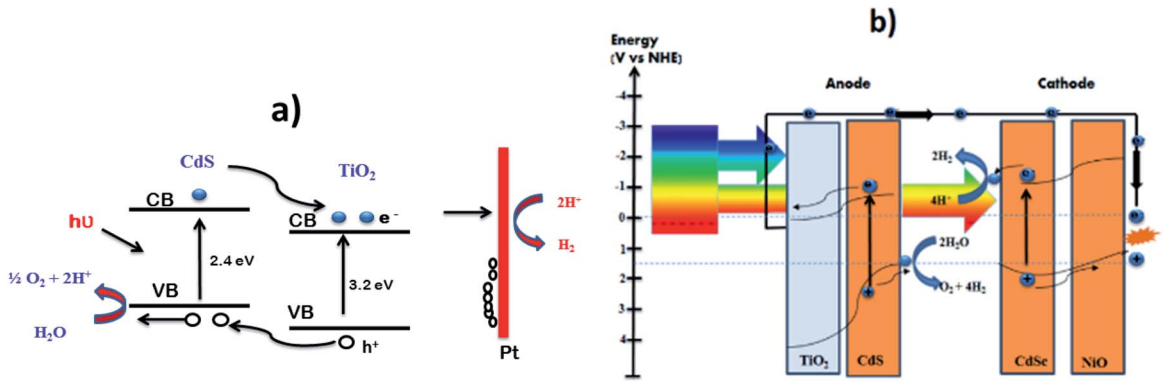

Fig. 12 Photoelectrochemical water splitting. (a) Mechanism of PEC water splitting by CdS–TiO_2 nanocomposite. Reproduced with permission from ref. 225 (b) photoelectrolysis cell consisting of CdS coupled TiO_2 photoanode and CdSe coupled NiO photocathode. Reproduced with permission from ref. 227.

visible light irradiation[229] and have attracted substantial attention worldwide. However, surface-modified CdS QDs also have important properties that make them versatile for photoelectrochemical water splitting.[230] The CB level of surface-modified CdS is higher than that of TiO_2, while the CB of CdSe is lower than that of TiO_2. Therefore, CdS NPs can be efficiently used for the transfer of electrons to TiO_2. But, because of its band gap energy of 2.25 eV in the bulk, the absorption range is limited to below 550 nm. Conversely, CdSe NPs have an extended absorption range (below 730 nm), but their CB level lies below the CB level of TiO_2. Advantageously, these materials have been used as co-sensitizers for TiO_2 films. However, poor performance was reported for the reversed structure, *i.e.*, TiO_2/CdSe/CdS. From knowledge of the Fermi levels of CdS and CdSe, a stepwise method for the construction of TiO_2/CdS/CdSe was described, which is an efficient electrode in photoelectrochemical cells for water splitting[118] (Fig. 13). The TiO_2–CdS nanohybrids displayed improved performance for water splitting compared to bare TiO_2. The cascade structure of TiO_2, sensitized with surface modified CdS and CdSe NPs, achieves the equilibrium of the band edge *via* alignment of the Fermi levels. Interfacial transfer of an electron between the QDs and TiO_2 is promoted, thus increasing the photocurrent.[231] ZnO nanowires and TiO_2 sensitized with surface-modified CdS and CdSe QDs represent electrodes with a high photocurrent density of 12 and 14.9 mA cm^{-2}, respectively, resulting in high efficiency for water splitting.

Other types of CdS-based heterojunction. Several other heterojunctions have been also reported, such as hexagonal–cubic CdS, and zinc blende–wurtzite $Zn_{1-x}Cd_xS$ solid solutions.[232–235] Others have been formed from two SCs, such as Au–TiO_2/CdS, CdS/CdSe, CdS/$Co_{0.85}Se$, *etc.*[201,236] The enhancement in the activity can, therefore, be attributed to the built-in-electric field thus created, which plays a key role in directing the charge flow. Also, both kinds of type-II heterojunctions can be combined into a single operation and have been efficiently used for electron survival, which has been achieved by coupling $PdP_{\sim 0.33}S_{\sim 1.67}$ with a nanocrystalline $Zn_{0.5}Cd_{0.5}S$ solid solution.[237] The heterojunction phase formed in $Zn_{0.5}Cd_{0.5}S$ suppressed charge recombination and afforded electrons for reduction reactions. Moreover, the phase formed between $PdP_{\sim 0.33}S_{\sim 1.67}$ and $Zn_{0.5}Cd_{0.5}S$ extracts electrons and encourages further charge survival, hence boosting the HER. The driving force for electron survival is the transfer of electrons between two SCs. Evidently, the greater the difference of energy, the more will be the driving force, even though the ability of an electron in this case to reduce the proton will be decreased. This conclusion has been confirmed by Zhong *et al.*, who found that there should be matching between the energy levels.[238] The loss in energy occurs between the two different CBs during electron transfer. If the CBs are at the same energy, the transfer will occur without any energy loss. Importantly, apart from the above heterojunctions, nanoscale interfacial contact is also significant for HER.[239] The ternary heterojunctions (In_2S_3/MoS_2/CdS composite) prepared by Jiang *et al.* are reported to be effective heterojunctions that compel holes from the CdS (VB) toward In_2S_3 owing to the difference in their VB energies, which impedes the photocorrosion of CdS, and therefore, enhances its stability.[240] In addition, the interphase between MoS_2 and CdS promotes the interfacial charge transfer, and hence reduces the recombination of photogenerated charges. The photocatalytic performance of this ternary heterojunction is much higher than the Pt deposited graphene oxide (GO)/CdS and reduced graphene oxide (RGO)/CdS nanohybrid. It is anticipated, that the sequential structural engineering and careful creation of the deposition site can significantly enhance the photocatalytic performance of the hybrid photocatalyst.

Recently, a core–shell nanowire of ZnO/ZnS/CdS/$CuInS_2$ was prepared which achieved a better photocurrent response (10.5 mA cm^{-2}) in the presence of Na_2S/Na_2SO_3 as an electrolyte with an IPCE of 57.7% at 480 nm at 0 V *vs.* Ag/AgCl.[241] The p–n junction designed between CdS and $CuInS_2$ maximizes the absorption of visible light and avoids the possibility of recombination. In Au-based junctions such as the CdS–Au–TiO_2 heterojunction (a detailed discussion of which follows in the next section), Au acts as a plasmonic sensitizer and charge facilitator, which results in a photocurrent response of 4.07 mA cm^{-2} at 0 V (*vs.* Ag/AgCl) with an STH efficiency of 2.8% under full arc irradiation.[134] The heterojunction allows the transfer of electrons and prolongs the lifetime of charges and so increases the rate of reaction. These photoelectrons were transferred from CdS *via* Au to TiO_2 at a lower incident wavelength (I < 525 nm). At longer wavelengths (525 nm–725 nm), however, CdS and TiO_2 were not excited and an extra plasmonic occurrence to transfer energy from the excited Au to TiO_2 takes place *via* a hot electron phenomenon as discussed earlier.

The above approach is somewhat different, but it has a very important and unique mechanism, which certainly offers an enhanced solar absorption capacity for photocatalytic water splitting. A heterojunction between CdS and Au (CdS/Au) exhibited excellent photocatalytic activity (*ca.* 4 mA cm^{-2} at 0 V *vs.* Ag/AgCl, Na_2S/Na_2SO_3 electrolyte) owing to the facile relocation of an electron from CdS to Au.[242] On the other hand, it has been reported that Au incorporation has an effect on H_2 production compared to Pt.[243] Tongying *et al.* fabricated some double-heterojunction nanowire (CdSe and CdSe/CdS NWs) photocatalysts decorated with Pt and achieved an H_2 generation rate of 435 μmol h^{-1} g^{-1}.[244]

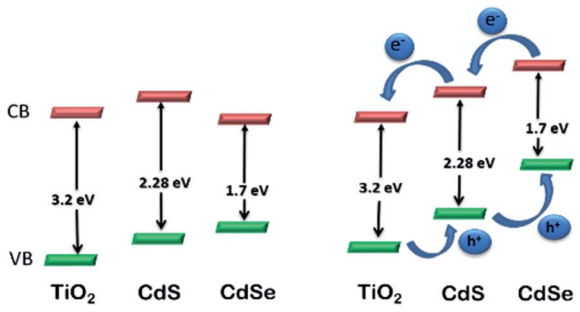

Fig. 13 Relative energy levels in TiO_2 photoelectrode co-sensitized with CdS and CdSe NPs. Reproduced with permission from ref. 118.

To develop a single junction from a core–shell structure, the coating of the SC is a good approach as it prolongs the lifetime of the charge carriers, which was achieved by hindering the influence of surface defects, which promote recombination, while in the double junction, the electrons are easily mobilized from the shell to the metal. Besides, the NiS/CdS p–n junction revealed notable H_2 photocatalytic activity because of the enhanced charge-transfer phenomenon at the junction of two SCs.[186] Similarly, a junction constructed between WS_2 and CdS displayed an excellent photocatalytic activity with an H_2 generation rate of 420 μmol h^{-1} g^{-1}, *i.e.*, a higher response than CdS but lower than that for a Pt/CdS electrode.[245]

CdS-based Z-scheme photocatalysis

As we have noted, heterojunctions play an important role in efficiently separating the charges. Unfortunately, the reduction capacity of the electron decreases as they move to a lower CB. As discussed earlier, Z-type natural photosynthesis is considered an effective mechanism for solar energy conversion. It consists of a two-step photoexcitation and comprises three types.[32–35] The first is "natural" photosynthesis for which the two SCs do not necessarily have to be in contact. The electron acceptor/donor (A/D) pairs need to transfer charges to each other, as in I^-/IO_3^- and Fe^{2+}/Fe^{3+}. The second and third types are A/D-free systems (known as solid-state Z-schemes). The second type contains the A/D pair which replaces the conductor as an electron mediator, while the third type has no need of a conductor.[246]

Zhang *et al.* have prepared a CdS/WO_3 heterojunction for the clean generation of H_2 *via* photolysis of water.[247] Interestingly, even though WO_3 cannot be used alone in water splitting, it enhances the photoactivity of CdS through a Z-scheme in the presence of lactate as an electron donor. An activity for H_2 production of 369 μmol h^{-1} g^{-1} using CdS/WO_3 (20 wt% CdS) was achieved (5 times greater than that of CdS) with lactic acid.[32] More recently, a RGO based ternary CdS/RGO/g-C_3N_4 hybrid system for H_2 generation by Z-scheme electron transportation has been designed.

By using a hydrothermal process, the two SCs exfoliated g-C_3N_4 nanosheets, and a CdS-coupled RGO can be coupled to construct a Z-scheme pathway. Compared to the bare CdS photocatalyst, the CdS/RGO/g-C_3N_4 hybrid showed more efficient H_2 generation owing to the better charge separation and photostability of the system. The RGO had a crucial role in channelling electrons between the interfaces of the two SCs through the Z-scheme route. An H_2 generation rate of 676.5 μmol h^{-1} g^{-1} with an AQE of 36.5% and 1980.2 μmol g^{-1} was achieved using the ternary hybrid material. Only an optimal amount of g-C_3N_4 (50 wt%) was loaded onto the hybrid system, as an excess amount beyond this limit (say, 70 wt%) would block the incoming light from the surface of CdS. The proposed Z-scheme charge transfer in the CdS/RGO/g-C_3N_4 composite was explained based on the band potentials of the two SCs and the electron mediation ability of the RGO. Under light irradiation, the electrons are readily promoted from the VBs to CBs of the two SCs (g-C_3N_4 and CdS). Consequently, the strong oxidation potential possessed by the VB of CdS (~1.88 eV) resulted predominantly in the oxidation of the sacrificial reagent. Meanwhile, the electrons from CdS flow into the RGO as CdS was grown *in situ* on the RGO nanosheets *via* a hydrothermal process. The Fermi level of the RGO and the CB of CdS were close in energy and so a very short distance for charge transfer was created. Subsequently, the VB holes of g-C_3N_4 were filled with electrons from the RGO (electron shift from CdS to g-C_3N_4 *via* RGO). As a consequence, the excess electrons residing in the CB of g-C_3N_4 reduced the H^+ ions of water to evolve H_2 gas.

Solid–solid contacts create a number of defects, to reduce which, the third type of Z-scheme has been developed. The electron mediator is removed to reduce the solid–solid interface contact area between the two SCs. Then, to augment electron transfer, a CdS/WO_3 nanohybrid has been prepared by Huang *et al.*[248] In this case, the function of the RGO is to facilitate the transfer of electrons and not to act as an electron mediator. Under light irradiation, both SCs generated electron–hole pairs where the CB electrons of CdS can readily move to the VB of WO_3 in the case where the electron mediator is absent. This transfer occurs due to the electrostatic interaction between CdS and WO_3 and operates as a Z-scheme.[249] The direct coupling of the components may not only avoid any back reactions and meanwhile can improve the reaction efficiency. Similarly, another simple technique was established for the preparation of CdS–Au–TiO_2 (an anisotropic nanojunction) on which Au was spatially fixed as an electron-transfer agent. This ternary system displays much higher activity than did either a single- and a two-component system. The higher activity achieved for the three-component system may be due to anisotropic electron movement between TiO_2 and CdS. As a consequence of the energy band of the three-component system (λ > 400 nm) (Fig. 14), the CB electrons reduce the methyl viologen (MV^{2+}) rather than being transferred to Au owing to the CdS size quantization.[250] The holes in the VB of CdS are subsequently filled by electrons from Au, as indicated by the red shift of λ_{max} (electron transfer I, Au → CdS). Meanwhile, at λ_{ex} > 300 nm, the

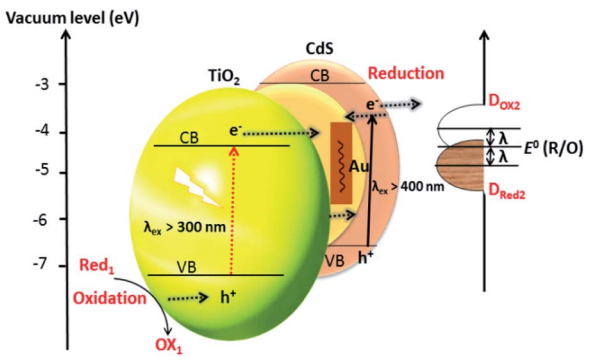

Fig. 14 Schematic energy diagram for the Z-scheme electron transfer mechanism. Energy band illustration of CdS–Au–TiO_2 system where E^0 (R/O) is the standard electrode potential of MV^+/MV^{2+} and D_{Red2} and D_{Ox2} illustrate the occupied and unoccupied states, respectively. *l* represent the reorganization energy. Reproduced with permission from ref. 250.

holes from the VB of TiO_2 have a strong ability to oxidize the solvent, while the electrons from the CB of TiO_2 flow into the Au (confirmed by the blue shift of λ_{max} for electron transfer II, TiO_2 → Au). The instantaneous electron transfers following I and II path (vectorial electron transfers) occur due to the excitation of both CdS and TiO_2 under the MV^{2+} reduction condition.

In view of the above discussion, Z-scheme photocatalysis has significant advantages because of the excellent reduction ability compared to heterojunctions. The available electrons reside in a higher CB rather than transferring to the lower one, which hinders the charge recombination very efficiently. It should be recognized that both heterojunction and Z-schemes have their own roles and specialties.

Given the above-mentioned approaches, the properties of some important CdS based photocatalysts are listed in Table 1 to provide an overall view of the modifications that have been made to CdS for the purpose of photocatalytic water splitting.

Charge utilization in CdS

After the generation and survival of photogenerated charges, the use of electrons for the HER is the overall objective of photocatalytic water splitting. The generated electrons reach the sites that generally reside on the surface of photocatalyst where they are in contact at the solid/liquid interface. The electrons on these sites transfer from the solid into the liquid phase to carry on the subsequent HER. In this section, we, therefore, discuss how to improve the use of photogenerated electrons.

Surface functionalization of CdS

Photocatalysis is a surface phenomenon. The photogenerated electrons reside on active sites that are on the photocatalyst or cocatalyst surface. A common approach is to load an optimized amount of cocatalyst (reduction cocatalyst) onto the photocatalyst. As mentioned before, co-catalysts play a dual role: (i) preventing recombination and (ii) acting as active sites either for activation of water molecules or for the reduction of protons. In the co-catalyst strategy, holes or electrons are scavenged by the co-catalysts once they are generated within the photocatalyst. For example, by introducing an oxidative co-catalyst, such as Co^{II}, not only is it possible to scavenge holes and hinder the recombination process but also provide an opportunity for the possible utilization of electrons.[26,28,59,79–83]

Another strategy is to extend the specific surface area of an SC (CdS) by decreasing its particle size. Unfortunately, very small-sized particles create additional problems. In this section, the functionalization of the CdS surface without the addition of additional materials will be discussed.

Lunawat *et al.* immobilized a CdS nanocatalyst on porous polymeric support (polystyrene).[299] The higher activity and longer life of coated CdS nanocatalyst in water splitting is the result of its hydrophobic nature. The number of active sites on the CdS surface can be increased by the immobilized polystyrene support. Thote *et al.* have prepared CdS NPs stabilized by the 2-D covalent organic framework (COF) to enhance photocatalytic H_2 production *via* water splitting.[300] The enhancement in activity has been ascribed to the presence of a p-conjugated polymer backbone and the abundant 2-D heterointerface and high surface-active sites, which act as efficient supports for stabilizing the photocatalyst and prolonging the lifetime of the photogenerated electrons. The effect of the coupling interface between CdS and the COF has been investigated. A comparison of the calculated flat-band potentials of CdS (0.64 V *vs.* NHE) and the COF (0.54 V, *vs.* NHE) suggests that CdS has a higher Fermi level than does the COF. The hybrid CdS–COF (90 : 10) has a flat-band potential of 0.59 V, which indicates that a new Fermi level has been designed between CdS and COF. In addition, the number of active sites formed by the preparation of this hybrid has increased markedly.

Wilker *et al.* have functionalized CdS NRs with mercaptocarboxylate surface-capping ligands to examine the role of ligands that passivate the sites of CdS with respect to transferring electrons to [FeFe] hydrogenase (from *Clostridium acetobutylicum*) for H_2 generation.[301]

The HER obtained matched the QE of the electron transfer. The authors suggested that H_2 production could be improved by introducing suitable surface-capping ligands that better-directed electrons to the target sites. Furthermore, Lin *et al.* demonstrated that poly(methyl methacrylate)–poly(methacrylic) (PMMA/PMAA) CdS nanocrystals have a shielded hybrid microsphere structure due to the formation of colloidal arrays.[302] They managed to prepare photonic crystals, which possessed both angular and spectral electromagnetic resonance structures. Through quantization effects, optical functionalization together with spectral control was achieved, *via* the *in situ* CdS nanocrystal growth on the surface of the microsphere.

Tailoring the pathway of reaction media

Once the electrons have crossed the solid/liquid interface, the ultimate goal is then to fix the pathway. It is understood that holes are utilized by either oxidation cocatalysts or by the scavengers thus allowing the free electrons to reduce the protons (H^+). This process is complex, leading to considerable conjecture regarding the mechanism. In almost all photocatalytic systems, a reduction cocatalyst, for example, is first loaded onto the photocatalyst (usually residing on the surface of the catalyst) forming a steric obstacle for the scavenger that suppressed electron–hole recombination. By tailoring the pathway, Simon *et al.* have reported that increasing the pH of the reaction media results in holes transferring from the photocatalyst to the scavenger (ethanol)[78] (Fig. 15a). The release and transfer of holes operate as a shuttle and the redox couple of $^{\bullet}OH/^{-}OH$ affords electrons for proton reduction, while the hydroxyl anions are regenerated through water dissociation. More importantly, through this shuttle mechanism, the slow hole scavenging pathway is substituted by two faster ones that involve redox mediator species. This redox shuttle technique greatly enhances the photocatalytic H_2 production compared to that for Ni/CdS (without ethanol). Hong *et al.* have prepared the ternary heterostructural system, ZnS–CuS–CdS, to use electrons more effectively[303] (Fig. 15b). They aimed to achieve synergy with

Table 1 CdS-based photocatalysts for H_2 generation from water splitting under visible-light irradiation

Photocatalyst	Mass (g)/volume (mL)	Light source (W/nm)	Sacrificial reagent	Cocatalysts	Rate (μmol h^{-1} g^{-1})	QE (%) 420 nm	Reference
CdS nanowire	0.1/100	500 Hg/<400	Na_2S/Na_2SO_3	Pt	≈60	—	251
Hexagonal CdS	0.1/200	300 Xe/≥420	Lactic acid	Pt	740.9	—	160
CdS	0.1/100	500 Hg/>420	Na_2S/Na_2SO_3	WC	≈1360	—	252
Hexagonal CdS	0.3/200	300 Xe/≥420	Na_2S/Na_2SO_3	Pt	1600	—	253
Nanoporous CdS	0.15/200	300 Xe/≥420	Na_2S/Na_2SO_3	Pt	600.34	—	254
Mesoporous CdS	0.1/50	400 Hg	Na_2S/Na_2SO_3	Pt	14 150	—	255
CdS microcrystal	0.03/40	500 Xe/≥400	Na_2S/Na_2SO_3	Pt	4600	—	256
CdS/ZnS	0.1/10	00 Ha UV	Na_2S/Na_2SO_3	—	≈40.5	—	257
CdS–$Zn_{1-x}Cd_xS$	0.05/80	350 Xe/>400	Na_2S/Na_2SO_3	—	≈2300	6.3	258
RGO–$Zn_{1-x}Cd_xS$	0.05/80	Solar simulator	Na_2S/Na_2SO_3	—	1820.4	23.4	259
CdS/ZnS/In_2S_3	0.015/320	300 Xe/>400	Na_2S/Na_2SO_3	—	8100	40.9	260
Pt–PdS–CdS	0.3/200	300 Xe/>420	Na_2S/Na_2SO_3	Pt	29 230	93	261
CdS–$AgGaS_2$	0.1	450 Hg/≥420	Na_2S/Na_2SO_3	Pt	2960	19.7	260
Ag_2S/CdS	0.1/120	Hg–Xe/>400	Na_2S/Na_2SO_3	Ag_2S & Pt	870.4	—	262
N-GR/CdS	0.2/300	300 Xe/>420	Na_2S/Na_2SO_3	—	1050		192
CdS/GR	0.02/80	350 Xe/≥420	Lactic acid	Pt	56 000	22.5	263
RGO–ZnCdS	0.05/80	Solar simulator	Na_2S/Na_2SO_3	—	1820.4	23.4	264
CdS/TiO_2 nanotube	0.15/300	300 Xe/≥420	Na_2S/Na_2SO_3	Pt	2080	43.4	76
CdS/TiO_2	0.1/50	350 Xe/≥400	Na_2S/Na_2SO_3	—	—	8.9	265
CdS/TiO_2	0.0125/25	450 Xe/>420	Na_2S/Na_2SO_3	Pt	6720	4.5	266
CdS/TiO_2	0.1/100	450 Hg/≥420	Na_2S/Na_2SO_3	Pt	≈110	—	267
PANI–PbS–CdS	0.2/200	300 Xe/>430	Na_2S/Na_2SO_3	—	16 600	—	268
CdS/TaON	0.2/200	300 Xe/=420	Na_2S/Na_2SO_3	Pt	3160.5	31	269
CdS/TNT	0.2/190	500 Xe/≥430	Na_2S/Na_2SO_3	Pt	1760.7	25.5	270
MWCNTS/CdS	0.035/100	300 Xe/≥420	Na_2S/Na_2SO_3	—	4980	—	271
$LaMnO_3$/CdS	0.1/60	300 Xe/≥420	Na_2S/Na_2SO_3	—	370.5	—	272
CdS/Re cellulose	0.05/100	250 Xe/≥420	Na_2S/Na_2SO_3	Pt	1320.3	—	273
CdS/$CdWO_4$	0.05/200	500 Xe	Na_2S/Na_2SO_3	—	1800.5	—	274
MoS_2/CdS	0.1/200	300 Xe	Lactic acid	MoS_2	≈5300	—	190
CdS/zeolite	0.1/50	400 Hg UV	Na_2S/Na_2SO_3	Pt	6000	—	75
Z–CdS	0.2/200	300 Xe	Na_2S/Na_2SO_3	RuO_2	≈6300	—	275
CdS/Ta_2O_5	0.05/50	Xe/400–800	Lactic acid	—	≈9000	—	276
CeO_2/CdS	0.05/100	300 Xe	Na_2S/Na_2SO_3	—	15 640	—	277
Z–CdS–Cd	0.1/300	300 Xe	Na_2S/Na_2SO_3	Pt	19 200	—	278
SrS/CdS	0.2/200	350 Xe/≥430	Na_2S/Na_2SO_3	—	—	2.85	69
NiO–CdS	0.2/50	500 halogen	Na_2S/Na_2SO_3	—	740.5	6	279
Sr/CdS	0.2/50	350 Xe	Na_2S/Na_2SO_3	—	1230	10	280
$Ni(OH)_2$/CdS	0.05/80	300 Xe/≥420	Triethalamine	Pt	5080.4	28	281
CdS/TaON	0.2/200	300 Xe/=420	Na_2S/Na_2SO_3	Pt	3160.5	31	282
CdS/Au/g-C_3N_4	0.5/60	300 Xe/>420	Methanol	Pt	19.02		283
CdS/g-C_3N_4	0.5/60	300 Xe/>420	Methanol	Pt	4152	4.3	283
CdS-QD's/g-C_3N_4	0.1/120	300 Xe/>400	Methanol	Pt	17.27	—	224
WS_2/CdS	0.1/200	300 Xe/≥400	Lactic acid	Pt	4200	—	245
WS_2–CdS	0.02/10	300 Xe/≥400	Lactic acid	—	2000	—	284
MoS_2/CdS	0.1/10	300 Xe/>420	Lactic acid	—	5400	—	190
NiO_x/CdS	0.1/100	300 Xe/>400	Na_2S/Na_2SO_3	—	590.8	8.6	285
CuS/CdS	0.2/200	500 Xe/>420	Na_2S/Na_2SO_3	—	3300	—	286
PdS/CdS	0.2/200	300 Xe/>430	Na_2S/Na_2SO_3	—	4450	—	176
NiS/CdS	0.05/80	300 Xe/>420	Na_2S/Na_2SO_3	NiS	1131	6.1	287
CdS/$K_2Ti_{3.9}Nb_{0.1}O_9$	0.1/20	300 Xe/>420	Na_2S/Na_2SO_3	—	4700	—	45
CdS–zeolite	0.1/50	400 Hg/>420	Na_2S/Na_2SO_3	—	102 (0.1 g_{cat})	—	75
CdS	0.2/100	Solar driven	—	—	340	—	288
$Co(OH)_2$/CdS	0.1/100	500 Xe/>420	—	Co	61	—	289
Ni/CdS	0.1/50	300 Xe/>420	$(NH_4)_2SO_3$	Ni	25 848	26.8	290
CdS/CNTs	0.1/180	350 Xe/>420	Na_2S/Na_2SO_3	—	794.6	—	291
CdS/CNTs	0.1/180	350 Xe/>420	Na_2S/Na_2SO_3	NiS	12 130	—	291
CdS/ZnS	0.1/10	500 halogen/>420	Na_2S/Na_2SO_3	—	45	—	69
CdSeZnS/ZTP	0.02/20	125 Hg/>420	Na_2S/Na_2SO_3	—	2142.7	9.6	292
ZnS–CuS–CdS	0.1/150	150 Xe/>420	—	—	837.6	—	293
GO/CdS	0.02/80	350 Xe/>420	—	Pt	1120	22.5	294
$Ni(OH)_2$–CdS/g-C_3N_4	0.001/20	300 Xe/>420	Na_2S/Na_2SO_3	Ni	115.18	16.7	295
Ni_h–CdS QDs	0.0008/10	500 Hg/>400	—	—	74.6	12.2	296

Table 1 (*Contd.*)

Photocatalyst	Mass (g)/volume (mL)	Light source (W/nm)	Sacrificial reagent	Cocatalysts	Rate (μmol h^{-1} g^{-1})	QE (%) 420 nm	Reference
$CdS/Pt/Ga_2O_3$	0.001/1	300 Xe/>420	—	—	995.8	43.6	297
$CdS/Pt/In_2O_3$	0.001/1	300 Xe/>420	—	—	1032.2	45.3	297
Au–Pt–CdS/SBA-15	0.1/20	500 halogen/>420	—	—	133.3		298

their system and, therefore, decrease the CdS content and increase the CuS content resulting in an appropriate improvement in the efficacy of the transfer of electrons to CuS. Optimizing the composition of this multi-component system will make possible the improved utilization of electrons for photolysis of water. Under illumination, the transfer of electrons from the VB of ZnS to CuS takes place, resulting in the partial reduction of CuS to Cu_2S. Meanwhile, because of the favourable VB position of CdS, electrons transfer first to ZnS and then to CuS *via* a cascade pathway.

Effect of sacrificial reagents

As has been emphasized above, it is difficult to achieve efficient photochemical H_2 production *via* water-splitting using TiO_2 and CdS without the addition of a sacrificial agent (hole scavenger/electron trapper). The anodic decomposition of CdS in the absence of a hole scavenger occurs at +0.32 V at pH 7 (eqn (2)).[10,52,304]

$$CdS + 2h^+ \rightarrow Cd^{2+} + S;\ E_{decomp} = +0.32\ V\ (NHE,\ pH\ 7) \quad (2)$$

The complex redox chemistry related to complete water splitting to afford gaseous H_2 evolution involves four electrons. There are two factors related to the use of sacrificial reagents.

First, in the case of using a hole scavenger, O_2 is not generated. Therefore, the reversible reaction for a generated water molecule is suppressed, which in turn, increases the H_2 production and avoids a gas separation stage. Secondly, the H_2 release rate can be reduced by the formation of an oxidized sacrificial reagent layer upon the surface of the photocatalyst.[305] In the presence of an electron-donor species like alcohol, S^{2-}, or SO_2^{3-}, however, the holes in the VB of the SC will oxidize the sacrificial reagent instead of corroding the photocatalyst, thus facilitating the reduction of water by the CB electrons.

Conversely, an electron-acceptor sacrificial reagent is irreversibly reduced by an electron (in the CB of the SC), which facilitates water oxidation by VB holes[10,78,185,306–308] (Fig. 16a). This phenomenon is related to the photodegradation of an organic contaminant oxidized by photogenerated holes. The most common sacrificial agents used are lactic acid,[165] formic acid,[52] S^{2-}/SO_3^{2-},[50] ethanol,[51] and some other organic and inorganic reagents.[10,53–55] Several organic compounds, such as organic acids, alcohol, and hydrocarbons are used as electron donors with CdS for photocatalytic H_2 generation.

Alcohols, such as ethanol and methanol, react irreversibly with the photogenerated holes, thus preventing photocorrosion of the photocatalyst as well as enhancing the probability of electron utilization, which in turn, increases the stability and QE of the photocatalyst. The continuous addition

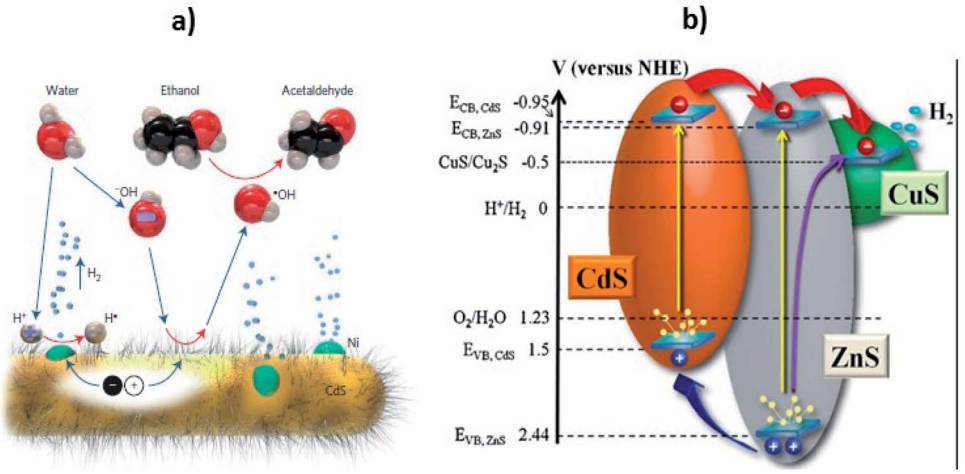

Fig. 15 (a) The proposed hole shuttle mechanism for H_2 generation over the cysteine-stabilized CdS nanorods. The hydroxyl anions scavenge the holes and carry away the positive charges which in turn oxidize the ethanol to acetaldehyde. The blue arrow represents the movement of species and red arrows denote a redox reaction. Reprinted with permission from ref. 78. (b) Charge transfer illustration in ZnS–CuS–CdS photocatalyst. Reprinted with permission from ref. 303.

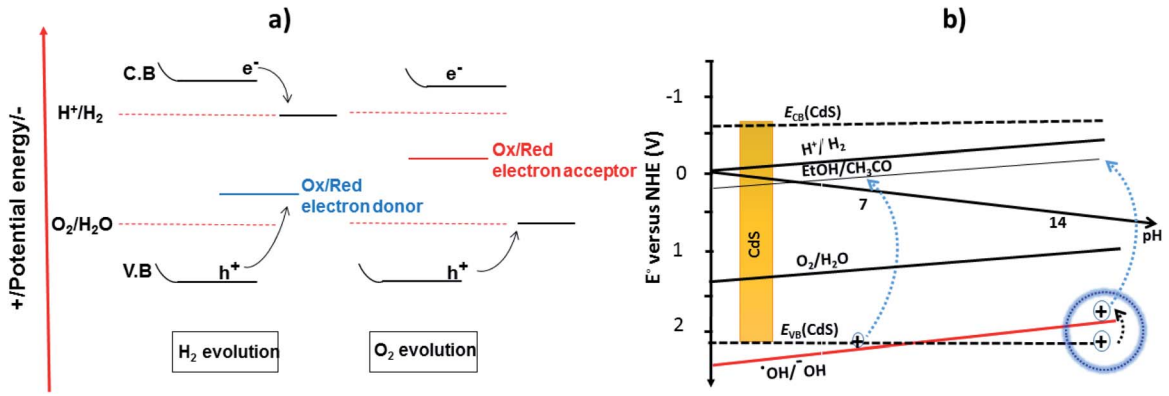

Fig. 16 Sacrificial reagents assisted photocatalytic water splitting. (a) Redox mediated reaction mechanism in the presence of sacrificial reagents. Reproduced with permission from ref. 307 and (b) the band edge position of CdS (CB and VB) and the relative redox potential of water, hydroxyl anion, and ethanol oxidation. Reproduced with permission from ref. 78.

of electron donors is required, however, for sustained H_2 generation, because of its continuous consumption.[78,309,310] This approach is somewhat limited at lower pH due to the reduction potential of protons *vs.* NHE. As mentioned earlier regarding the report of Simon *et al.*, the scavenging of holes from CdS (in the VB) is based on the $^{\cdot}OH/OH^-$ redox couple, functioning as a shuttle.[78] This redox-mediated mechanism significantly boosts the H_2 production over Ni/CdS (in the presence of ethanol as a scavenger). Moreover, hole scavenging from the VB of CdS by OH^- ions are only favorable at high pH (Fig. 16b).

Harada *et al.* have tested the oxidation ability of CdS using several sacrificial reagents and discovered that not all the sacrificial reagent is prone to oxidation by the photogenerated holes.[311] The main point is the compatibility of the oxidation potentials of the photocatalyst (VB potential) and sacrificial reagent. The higher the oxidation potential of the VB, the easier the species can be oxidized by the photogenerated holes. Zong *et al.* developed a MoS_2/CdS photocatalytic system for H_2 generation using different sacrificial agents with their activity order being lactic acid > glycerol > glycol > ethanol > methanol.[312] Inorganic electron donors such as sulfide (S^{2-}) and sulfite (SO_3^{2-}) ions can also act as hole scavengers. These two sulfur-containing anions allow electrons to be utilized in the HER and are the most commonly used sacrificial agents. As discussed earlier, in the presence of electron donor species, CdS is considered to be an efficient photocatalyst for the generation of H_2 from aqueous systems.[174,223,313–316] The VB level of CdS is positive enough (+2.2 V *vs.* NHE) for the oxidation of sulfur-containing compounds.[317] As mentioned before, there are two advantages of using S^{2-} and/or SO_3^{2-} as hole scavengers for CdS over alcohols: (i) they are easily oxidized by VB holes, which reduces the undesired anodic photo corrosion and (ii) the dissolved Cd^{2+} in a solution can reform CdS upon reaction with S^{2-}. In aqueous methanol solution, however, it is not practical to reform CdS. The very high QE (93%) was achieved upon employing Pt–PdS/CdS as the photocatalyst in the presence of S^{2-}/SO_3^{2-}.[318] Berr *et al.* applied transient absorption spectroscopy on colloidal Pt-decorated CdS nanorods in the presence and absence of Na_2SO_3 as the hole scavenger.[319] Notably, the migration of photoelectrons from the CB of CdS to the active site of Pt was slow without the use of a hole scavenger and resulted in no significant H_2 generation. The possible mechanistic steps for the H_2 production in the presence of S^{2-}/SO_3^{2-} as electron-donor sacrificial agents are given in eqn (3)–(8).

$$2H_2O + 2e^- \rightarrow H_2 + 2OH^- \quad (3)$$

$$SO_3^{2-} + 2OH^- + 2h^+ \rightarrow SO_4^{2-} + H_2O \quad (4)$$

$$S_2O_3^{2-} + 2h^+ \rightarrow S_2O_6^{2-} \quad (5)$$

$$2S^{2-} + 2h^+ \rightarrow S_2^{2-} \quad (6)$$

$$SO_3^{2-} + S^{2-} + 2h^+ \rightarrow S_2O_3^{2-} \quad (7)$$

$$S_2^{2-} + SO_3^{2-} \rightarrow S_2O_3^{2-} + S^{2-} \quad (8)$$

Some inorganic ions also act as sacrificial agents for a CdS photocatalyst, such as Ce^{3+}, Fe^{2+}, Ni^{2+}, and I^-.[78,320] Unfortunately, it is necessary constantly to add these sacrificial agents to keep the reaction viable, which is both inconvenient and not cost-effective. Therefore, the replacement of inorganic sacrificial agents with organic ones is the best approach to generate H_2 from water using a CdS photocatalyst.

The choice of electron donors as sacrificial agents for water splitting is quite extensive when compared to the range of possible electron acceptors. Nevertheless, electron acceptor agents have their own advantages, but they must be used where the photocatalyst is stable enough to oxidation.

Moreover, there is some concern with using only an oxidation process. As an example, Ag^+ has been employed an electron acceptor (eqn (9)–(11)).

$$4h^+ + 2H_2O \xrightarrow{h\nu} O_2 + 4H_{aq}^+ \quad (9)$$

$$4e^- + 4Ag^+ \xrightarrow{h\nu} 4Ag^0 \quad (10)$$

$$nAg^0 \xrightarrow{h\nu} Ag_n^0 \quad (11)$$

Here, Ag^+ is acting as an electron scavenging agent. CdS is prone to oxidation[321] and, even more so, in the presence of electron acceptor agents, and it will certainly be susceptible to degradation.The generation of molecular oxygen is accompanied by metallic silver nanocontacts (Ag_n^0) on the surface of the SC. So, sacrificial electron acceptors are in general not particularly beneficial for photocatalytic H_2 generation using CdS-based photocatalysts.

Conclusions and future perspective

Photocatalysis is a highly important multifunctional technology in the areas of energy and environmental remediation, especially photocatalytic H_2 production and CO_2 reduction.[28,322] Solar H_2 generation from water is a key strategy in addressing the world's energy shortage by utilising the ample solar energy directly in the form of molecular hydrogen, a green fuel.[323,324] Although photocatalytic technology has grown and been applied to using solar energy to generate H_2 and other fuels, there are still challenges with its efficiency. As we have shown in this review, to enhance the efficiency of this technology, the three critical steps *i.e.*, charge generation, charge survival, and its proper utilization need significant development, both for solar light conversion to electricity and photocatalytic H_2 production. Among these, the first cornerstone is to improve the light absorption ability of the material for effective charge generation. CdS is basically a visible light-responsive photocatalyst; its absorption properties can be modified up to the full visible range or the IR region. As is evident from many literature reports, the strategies of combining two photocatalysts or plasmonic electron generation have been found to be very successful in enhancing the light absorption capacities of photocatalyst. Moreover, deliberately introducing structural defects and chemical impurities also widen the spectral response of CdS.

Suppression of electron–hole recombination is the key to all photocatalytic processes and is crucial for charge survival. The strategies recommended for reducing the rate of charge recombination in CdS include: (i) anisotropic induction and morphology engineering, which effectively suppresses charge recombination; (ii) co-catalyst incorporation, which extracts electrons from the CB level of the photocatalyst; (iii) induced heterojunction formation, which pushes the charges in opposite directions; and (iv) Z-scheme photocatalysis which, like natural photosynthesis, involves a two-step photoexcitation and also hinders the recombination process and promotes charge separation as do heterojunctions. However, the reduction ability of an electron and the prevention of the backward reaction of water splitting is often better in Z-scheme photocatalysis than in the heterojunctions. Moreover, elevating the position of the CB level through crystal engineering has also proved a highly feasible approach to improve the ability (for reduction of a proton) of the photogenerated electrons. Furthermore, to increase the efficacy of the photocatalyst, the search for cost-effective and efficient cocatalysts should be continued to replace Pt-based cocatalysts. After these two processes, presumably the charges especially electrons reach the sites and are utilized for the HER. The main protagonists are electrons, which are emitted from the photocatalyst and enter smoothly into the solid/liquid interface. Surface functionalization for charge transportation can be achieved by surface modification (an increased number of active sites) and by introducing foreign materials having high conductivities. Currently, the available efficiency of CdS-based photocatalysts is relatively low due to the fast recombination of the electron–hole pair, the backward reaction, and the photo-corrosion effect. To make these processes more feasible, the continual addition of electron-donor species into the reaction medium is needed. These electron-donor agents irreversibly consume photogenerated holes and allow electrons to be used for proton reduction as well as hindering the undesired charge recombination phenomenon. Interestingly, the use of biomass (low-cost and renewable source) from animals and plants may well provide sacrificial reagents for water-splitting, at almost no cost; and both H_2 production and waste-water treatment could be performed in parallel.

Finally, all the above strategies play key roles in improving the performance of CdS-based photocatalysts. There are several CdS-based photocatalysts that have not yet been tested for H_2 generation from water; more information on them is still needed. In addition, the reaction kinetics and molecular mechanisms must be considered carefully when further developing CdS-based photocatalytic systems. Nevertheless, it is vitally important to pursue such an ambitious goal for meeting future energy needs. The industrial application of photocatalytic H_2 production will also require comprehensive studies to scale-up laboratory studies and improve the low photocatalytic efficiency of the photocatalysts. The design of a robust and efficient photocatalytic system remains a major future challenge. This review has indicated where some of the fundamental developments will be needed.

List of abbreviations

CB	Conduction band
VB	Valence band
H_2	Hydrogen
CO_2	Carbon dioxide
SC	Semiconductor
NHE	Normal hydrogen electrode
NMs	Nanomaterials
NPs	Nanoparticles
NCs	Nanocrystals
NTs	Nanotubes
HER	Hydrogen evolution reaction
RHE	Reversible hydrogen electrode
DFT	Density functional theory
RGO	Reduced graphene oxide
GO	Graphene oxide
XPS	X-ray photoelectron spectroscopy
SEM	Scanning electron microscopy
FESEM	Field emission scanning electron microscopy
STEM	Scanning tunnelling electron microscopy

TEM	Transmission electron microscopy
HRTEM	High resolution transmission electron microscopy
TDA	Transient differential absorption
A/D pair	Electron acceptor/donor
ZTP	Zirconium titanium phosphate
QD	Quantum dot
IPCE	Incident-photon-to-current-conversion efficiency
LSPR	Localized surface plasmon resonance
CTAB	Cetyltrimethylammonium bromide
AQY	Apparent quantum yield
AQE	Apparent quantum efficiency
EQY	External quantum yield
QE	Quantum efficiency
HT	Head-to-tail
P3HT	Poly-(3-hexylthiophene-2,5-diyl)
NCs	Nanocubes
NOTs	Nanooctahedrons
ECSA	Electrochemical active surface area
POM	Polyoxometalate
PSRD	Plasma sputtering reaction
PLD	Pulsed laser deposition
IPCE	Incident photon-to-current conversion efficiency
COF	Covalent organic frame work
PMMA/ PMAA	Poly-methyl methacrylate–poly-methacrylic
TMBs	Transition metal borides
NIR	Near infrared
UV	Ultraviolet
ITO	Indium tin oxide
CQDs	Carbon quantum dots
2D	Two dimensional
1D	One dimensional
PL	Photoluminescence
STH	Solar-to-hydrogen efficiency
PEC	Photoelectrochemical

Conflicts of interest

There are no conflicts to declare.

Acknowledgements

We acknowledge the financial support from the Higher Education Commission of Pakistan.

Notes and references

1 N. Panwar, S. Kaushik and S. Kothari, *Renewable Sustainable Energy Rev.*, 2011, **15**, 1513–1524.
2 F. E. Osterloh, *Chem. Soc. Rev.*, 2013, **42**, 2294–2320.
3 J. Kundu, S. Khilari and D. Pradhan, *ACS Appl. Mater. Interfaces*, 2017, **9**, 9669–9680.
4 C.-H. Liao, C.-W. Huang and J. Wu, *Catalysts*, 2012, **2**, 490–516.
5 U. EIA, US Energy Information Administration, Washington, DC, 2013, pp. 60–62.
6 N. S. Lewis and D. G. Nocera, *Proc. Natl. Acad. Sci. U. S. A.*, 2006, **103**, 15729–15735.
7 N. S. Lewis, G. Crabtree, A. J. Nozik, M. R. Wasielewski, P. Alivisatos, H. Kung and R. Ellingson, *Basic Research Needs for Solar Energy Utilization, Report of the Basic Energy Sciences Workshop on Solar Energy Utilization*, DOESC (USDOE Office of Science (SC)), 2005.
8 N. Panwar, S. Kaushik and S. Kothari, *Renewable Sustainable Energy Rev.*, 2011, **15**, 1513–1524.
9 Z. Yang, J. Zhang, M. C. Kintner-Meyer, X. Lu, D. Choi, J. P. Lemmon and J. Liu, *Chem. Rev.*, 2011, **111**, 3577–3613.
10 X. Chen, S. Shen, L. Guo and S. S. Mao, *Chem. Rev.*, 2010, **110**, 6503–6570.
11 A. Züttel, A. Remhof, A. Borgschulte and O. Friedrichs, *Philos. Trans. R. Soc., A*, 2010, **368**, 3329–3342.
12 I. Roger, M. A. Shipman and M. D. Symes, *Nat. Rev. Chem.*, 2017, **1**, 0003.
13 Y. Tachibana, L. Vayssieres and J. R. Durrant, *Nat. Photonics*, 2012, **6**, 511.
14 X. Zou and Y. Zhang, *Chem. Soc. Rev.*, 2015, **44**, 5148–5180.
15 W. Brattain and C. Garrett, *Bell Labs Tech. J.*, 1955, **34**, 129–176.
16 H. Gerischer, *J. Electrochem. Soc.*, 1966, **113**, 1174–1182.
17 Y. V. Pleskov and Y. Y. Gurevich, *Semiconductor photoelectrochemistry*, 1986.
18 A. J. Bard, *J. Photochem.*, 1979, **10**, 59–75.
19 A. J. Nozik, *Annu. Rev. Phys. Chem.*, 1978, **29**, 189–222.
20 A. Fujishima and K. Honda, *Nature*, 1972, **238**, 37–38.
21 A. Fujishima, *Nature*, 1972, **238**, 37–38.
22 A. Kudo and Y. Miseki, *Chem. Soc. Rev.*, 2009, **38**, 253–278.
23 J. Ran, J. Zhang, J. Yu, M. Jaroniec and S. Z. Qiao, *Chem. Soc. Rev.*, 2014, **43**, 7787–7812.
24 M. Matsuoka, M. Kitano, M. Takeuchi, K. Tsujimaru, M. Anpo and J. M. Thomas, *Catal. Today*, 2007, **122**, 51–61.
25 T. Hisatomi, J. Kubota and K. Domen, *Chem. Soc. Rev.*, 2014, **43**, 7520–7535.
26 A. Kudo and Y. Miseki, *Chem. Soc. Rev.*, 2009, **38**, 253–278.
27 M. B. Wilker, K. J. Schnitzenbaumer and G. Dukovic, *Isr. J. Chem.*, 2012, **52**, 1002–1015.
28 K. Maeda and K. Domen, *J. Phys. Chem. Lett.*, 2010, **1**, 2655–2661.
29 K. Maeda, T. Takata, M. Hara, N. Saito, Y. Inoue, H. Kobayashi and K. Domen, *J. Am. Chem. Soc.*, 2005, **127**, 8286–8287.
30 Y. Lee, H. Terashima, Y. Shimodaira, K. Teramura, M. Hara, H. Kobayashi, K. Domen and M. Yashima, *J. Phys. Chem. C*, 2007, **111**, 1042–1048.
31 S. Ma, J. Xie, J. Wen, K. He, X. Li, W. Liu and X. Zhang, *Appl. Surf. Sci.*, 2017, **391**, 580–591.
32 L. J. Zhang, S. Li, B. K. Liu, D. J. Wang and T. F. Xie, *ACS Catal.*, 2014, **4**, 3724–3729.
33 P. Zhou, J. Yu and M. Jaroniec, *Adv. Mater.*, 2014, **26**, 4920–4935.
34 W. Li, C. Feng, S. Dai, J. Yue, F. Hua and H. Hou, *Appl. Catal., B*, 2015, **168**, 465–471.
35 B. Qiu, Q. Zhu, M. Du, L. Fan, M. Xing and J. Zhang, *Angew. Chem.*, 2017, **129**, 2728–2732.

36 J. Low, C. Jiang, B. Cheng, S. Wageh, A. A. Al-Ghamdi and J. Yu, *Small Methods*, 2017, **1**, 1700080.
37 K. Sayama, K. Mukasa, R. Abe, Y. Abe and H. Arakawa, *Chem. Commun.*, 2001, 2416–2417.
38 H. Kato, M. Hori, R. Konta, Y. Shimodaira and A. Kudo, *Chem. Lett.*, 2004, **33**, 1348–1349.
39 M. Ni, M. K. Leung, D. Y. Leung and K. Sumathy, *Renewable Sustainable Energy Rev.*, 2007, **11**, 401–425.
40 A. L. Linsebigler, G. Lu and J. T. Yates Jr, *Chem. Rev.*, 1995, **95**, 735–758.
41 A. Fujishima, X. Zhang and D. A. Tryk, *Surf. Sci. Rep.*, 2008, **63**, 515–582.
42 S. Kaur and V. Singh, *J. Hazard. Mater.*, 2007, **141**, 230–236.
43 R. M. Navarro Yerga, M. C. Álvarez Galván, F. Del Valle, J. A. Villoria de la Mano and J. L. Fierro, *ChemSusChem*, 2009, **2**, 471–485.
44 R. Abe, *J. Photochem. Photobiol., C*, 2010, **11**, 179–209.
45 W. Shangguan and A. Yoshida, *J. Phys. Chem. B*, 2002, **106**, 12227–12230.
46 H. Yin, Y. Wada, T. Kitamura and S. Yanagida, *Environ. Sci. Technol.*, 2001, **35**, 227–231.
47 M. Matsumura, S. Furukawa, Y. Saho and H. Tsubomura, *J. Phys. Chem.*, 1985, **89**, 1327–1329.
48 J. F. Reber and M. Rusek, *J. Phys. Chem.*, 1986, **90**, 824–834.
49 L. Amirav and A. P. Alivisatos, *J. Phys. Chem. Lett.*, 2010, **1**, 1051–1054.
50 J. S. Jang, S. M. Ji, S. W. Bae, H. C. Son and J. S. Lee, *J. Photochem. Photobiol., A*, 2007, **188**, 112–119.
51 S. Y. Ryu, W. Balcerski, T. Lee and M. R. Hoffmann, *J. Phys. Chem. C*, 2007, **111**, 18195–18203.
52 Y. J. Zhang, L. Zhang and S. Li, *Int. J. Hydrogen Energy*, 2010, **35**, 438–444.
53 X. Zong, G. Wu, H. Yan, G. Ma, J. Shi, F. Wen, L. Wang and C. Li, *J. Phys. Chem. C*, 2010, **114**, 1963–1968.
54 J. Jin, J. Yu, G. Liu and P. K. Wong, *J. Mater. Chem. A*, 2013, **1**, 10927–10934.
55 Y. Li, Y. Hu, S. Peng, G. Lu and S. Li, *J. Phys. Chem. C*, 2009, **113**, 9352–9358.
56 M. F. Kuehnel, D. W. Wakerley, K. L. Orchard and E. Reisner, *Angew. Chem., Int. Ed.*, 2015, **54**, 9627–9631.
57 W.-T. Yao, S.-H. Yu, S.-J. Liu, J.-P. Chen, X.-M. Liu and F.-Q. Li, *J. Phys. Chem. B*, 2006, **110**, 11704–11710.
58 X. Song, W. Yao, B. Zhang and Y. Wu, *Int. J. Photoenergy.*, 2012, 1–5.
59 S. J. Moniz, S. A. Shevlin, D. J. Martin, Z.-X. Guo and J. Tang, *Energy Environ. Sci.*, 2015, **8**, 731–759.
60 J. R. Darwent and G. Porter, *J. Chem. Soc., Chem. Commun.*, 1981, 145–146.
61 M. Matsumura, Y. Saho and H. Tsubomura, *J. Phys. Chem.*, 1983, **87**, 3807–3808.
62 F. Del Valle, A. Ishikawa, K. Domen, J. V. de La Mano, M. Sánchez-Sánchez, I. González, S. Herreras, N. Mota, M. Rivas and M. Á. Galván, *Catal. Today*, 2009, **143**, 51–56.
63 E. Borgarello, J. Kiwi, M. Graetzel, E. Pelizzetti and M. Visca, *J. Am. Chem. Soc.*, 1982, **104**, 2996–3002.
64 F. Zuo, L. Wang, T. Wu, Z. Zhang, D. Borchardt and P. Feng, *J. Am. Chem. Soc.*, 2010, **132**, 11856–11857.
65 R. Niishiro, R. Konta, H. Kato, W.-J. Chun, K. Asakura and A. Kudo, *J. Phys. Chem. C*, 2007, **111**, 17420–17426.
66 R. Asahi, T. Morikawa, T. Ohwaki, K. Aoki and Y. Taga, *Science*, 2001, **293**, 269–271.
67 X. Li, N. Kikugawa and J. Ye, *Adv. Mater.*, 2008, **20**, 3816–3819.
68 A. Kongkanand, K. Tvrdy, K. Takechi, M. Kuno and P. V. Kamat, *J. Am. Chem. Soc.*, 2008, **130**, 4007–4015.
69 A. Deshpande, P. Shah, R. Gholap and N. M. Gupta, *J. Colloid Interface Sci.*, 2009, **333**, 263–268.
70 C. Xing, Y. Zhang, W. Yan and L. Guo, *Int. J. Hydrogen Energy*, 2006, **31**, 2018–2024.
71 S. Pelet, J.-E. Moser and M. Grätzel, *J. Phys. Chem. B*, 2000, **104**, 1791–1795.
72 G. K. Mor, K. Shankar, M. Paulose, O. K. Varghese and C. A. Grimes, *Nano Lett.*, 2006, **6**, 215–218.
73 J. Xie, J. Zhang, S. Li, F. Grote, X. Zhang, H. Zhang, R. Wang, Y. Lei, B. Pan and Y. Xie, *J. Am. Chem. Soc.*, 2013, **135**, 17881–17888.
74 M. Salari, S. H. Aboutalebi, A. Aghassi, P. Wagner, A. J. Mozer and G. G. Wallace, *Phys. Chem. Chem. Phys.*, 2015, **17**, 5642–5649.
75 M. Sathish, B. Viswanathan and R. Viswanath, *Int. J. Hydrogen Energy*, 2006, **31**, 891–898.
76 C. Li, J. Yuan, B. Han, L. Jiang and W. Shangguan, *Int. J. Hydrogen Energy*, 2010, **35**, 7073–7079.
77 J. Yang, D. Wang, H. Han and C. Li, *Acc. Chem. Res.*, 2013, **46**, 1900–1909.
78 T. Simon, N. Bouchonville, M. J. Berr, A. Vaneski, A. Adrović, D. Volbers, R. Wyrwich, M. Döblinger, A. S. Susha and A. L. Rogach, *Nat. Mater.*, 2014, **13**, 1013–1018.
79 M. A. Khan, Z.-u. Rehman, J. A. Nasir, M. Hafeez, M. Arshad, N. Z. Ali, I. F. Teixieira and I. McPherson, *ChemSusChem*, 2018, **11**, 2587–2592.
80 M. G. Walter, E. L. Warren, J. R. McKone, S. W. Boettcher, Q. Mi, E. A. Santori and N. S. Lewis, *Chem. Rev.*, 2010, **110**, 6446–6473.
81 M. Ni, M. K. Leung, D. Y. Leung and K. Sumathy, *Renewable Sustainable Energy Rev.*, 2007, **11**, 401–425.
82 J. P. McEvoy and G. W. Brudvig, *Chem. Rev.*, 2006, **106**, 4455–4483.
83 P. Du and R. Eisenberg, *Energy Environ. Sci.*, 2012, **5**, 6012–6021.
84 G. Wang, X. Yang, F. Qian, J. Z. Zhang and Y. Li, *Nano Lett.*, 2010, **10**, 1088–1092.
85 X. Yue, S. Yi, R. Wang, Z. Zhang and S. Qiu, *Sci. Rep.*, 2016, **6**, 22268.
86 Y. Xu and M. A. Schoonen, *Am. Mineral.*, 2000, **85**, 543–556.
87 L. Cheng, Q. Xiang, Y. Liao and H. Zhang, *Energy Environ. Sci.*, 2018, **11**, 1362.
88 D. Meissner, R. Memming and B. Kastening, *J. Phys. Chem.*, 1988, **92**, 3476–3483.
89 W. Shangguan and A. Yoshida, *J. Phys. Chem. B*, 2002, **106**, 12227–12230.
90 T. Hirai and Y. Bando, *J. Colloid Interface Sci.*, 2005, **288**, 513–516.

91 Y. Yang, Y. Zhang, Z. Fang, L. Zhang, Z. Zheng, Z. Wang, W. Feng, S. Weng, S. Zhang and P. Liu, *ACS Appl. Mater. Interfaces*, 2017, **9**, 6950–6958.
92 Y. Zhong, G. Zhao, F. Ma, Y. Wu and X. Hao, *Appl. Catal., B*, 2016, **199**, 466–472.
93 A. Wu, C. Tian, Y. Jiao, Q. Yan, G. Yang and H. Fu, *Appl. Catal., B*, 2017, **203**, 955–963.
94 J. Hou, C. Yang, Z. Wang, S. Jiao and H. Zhu, *RSC Adv.*, 2012, **2**, 10330–10336.
95 J. Yu, Y. Yu, P. Zhou, W. Xiao and B. Cheng, *Appl. Catal., B*, 2014, **156**, 184–191.
96 H. Yu, X. Huang, P. Wang and J. Yu, *J. Phys. Chem. C*, 2016, **120**, 3722–3730.
97 W. Zhang, Y. Wang, Z. Wang, Z. Zhong and R. Xu, *Chem. Commun.*, 2010, **46**, 7631–7633.
98 D. Meissner, R. Memming and B. Kastening, *Chem. Phys. Lett.*, 1983, **96**, 34–37.
99 D. Meissner, R. Memming, L. Shuben, S. Yesodharan and M. Grätzel, *Ber. Bunsen-Ges. Phys. Chem.*, 1985, **89**, 121–124.
100 T. Torimoto, M. Hashitani, T. Konishi, K.-i. Okazaki, T. Shibayama and B. Ohtani, *J. Nanosci. Nanotechnol.*, 2009, **9**, 506–513.
101 Y. Hu, X. Gao, L. Yu, Y. Wang, J. Ning, S. Xu and X. W. D. Lou, *Angew. Chem.*, 2013, **125**, 5746–5749.
102 M.-Q. Yang, C. Han and Y.-J. Xu, *J. Phys. Chem. C*, 2015, **119**, 27234–27246.
103 Y. Bessekhouad, N. Chaoui, M. Trzpit, N. Ghazzal, D. Robert and J. Weber, *J. Photochem. Photobiol., B*, 2006, **183**, 218–224.
104 L. Ma, M. Liu, D. Jing and L. Guo, *J. Mater. Chem. A*, 2015, **3**, 5701–5707.
105 A. V. Isarov and J. Chrysochoos, *Langmuir*, 1997, **13**, 3142–3149.
106 L. Spanhel, M. Haase, H. Weller and A. Henglein, *J. Am. Chem. Soc.*, 1987, **109**, 5649–5655.
107 Y. Zhu, Z. Chen, T. Gao, Q. Huang, F. Niu, L. Qin, P. Tang, Y. Huang, Z. Sha and Y. Wang, *Appl. Catal., B*, 2015, **163**, 16–22.
108 H. Yan, J. Yang, G. Ma, G. Wu, X. Zong, Z. Lei, J. Shi and C. Li, *J. Catal.*, 2009, **266**, 165–168.
109 V. M. Daskalaki, M. Antoniadou, G. Li Puma, D. I. Kondarides and P. Lianos, *Environ. Sci. Technol.*, 2010, **44**, 7200–7205.
110 P. Srivastava, P. Kumar and K. Singh, *J. Nanopart. Res.*, 2011, **13**, 5077.
111 Z. Gao, N. Liu, D. Wu, W. Tao, F. Xu and K. Jiang, *Appl. Surf. Sci.*, 2012, **258**, 2473–2478.
112 S. Chandramohan, A. Kanjilal, J. K. Tripathi, S. N. Sarangi, R. Sathyamoorthy and T. Som, *J. Appl. Phys.*, 2009, **105**, 123507.
113 M. V. Kovalenko, R. D. Schaller, D. Jarzab, M. A. Loi and D. V. Talapin, *J. Am. Chem. Soc.*, 2012, **134**, 2457–2460.
114 Z. Ning, H. Tian, C. Yuan, Y. Fu, H. Qin, L. Sun and H. Ågren, *Chem. Commun.*, 2011, **47**, 1536–1538.
115 A. Nemchinov, M. Kirsanova, N. N. Hewa-Kasakarage and M. Zamkov, *J. Phys. Chem. C*, 2008, **112**, 9301–9307.
116 M. Braun, C. Burda and M. A. El-Sayed, *J. Phys. Chem. A*, 2001, **105**, 5548–5551.
117 Y. L. Lee and Y. S. Lo, *Adv. Funct. Mater.*, 2009, **19**, 604–609.
118 Y.-L. Lee, C.-F. Chi and S.-Y. Liau, *Chem. Mater.*, 2010, **22**, 922–927.
119 A. K. Gupta and R. Kripal, *Spectrochim. Acta, Part A*, 2012, **96**, 626–631.
120 Z. K. Heiba, M. B. Mohamed and N. Imam, *J. Alloys Compd.*, 2015, **618**, 280–286.
121 S. Huang, Y. Lin, J. Yang, X. Li, J. Zhang, J. Yu, H. Shi, W. Wang and Y. Yu, *RSC Adv.*, 2013, **3**, 20782–20792.
122 H. Duan and Y. Xuan, *Sol. Energy Mater. Sol. Cells*, 2014, **121**, 8–13.
123 L. A. González, I. Carreón-Moncada and M. A. Quevedo-López, *Mater. Lett.*, 2017, **192**, 161–164.
124 B. A. Korgel and H. G. Monbouquette, *Langmuir*, 2000, **16**, 3588–3594.
125 G. Wang, X. Yang, F. Qian, J. Z. Zhang and Y. Li, *Nano Lett.*, 2010, **10**, 1088–1092.
126 N. M. Vuong, J. L. Reynolds, E. Conte and Y.-I. Lee, *J. Phys. Chem. C*, 2015, **119**, 24323–24331.
127 K. Parida, N. Biswal, D. Das and S. Martha, *Int. J. Hydrogen Energy*, 2010, **35**, 5262–5269.
128 M. B. Dines, P. M. DiGiacomo, K. P. Callahan, P. C. Griffith, R. H. Lane and R. E. Cooksey, in *Chemically Modified Surfaces in Catalysis and Electrocatalysis*, ed. J. S. Miller, ACS Symposium Series 192, ACS, Washington, DC, 1982, p. 223.
129 R. Jiang, B. Li, C. Fang and J. Wang, *Adv. Mater.*, 2014, **26**, 5274–5309.
130 H. Duan and Y. Xuan, *Phys. E*, 2011, **43**, 1475–1480.
131 K. Wu, W. E. Rodríguez-Córdoba, Y. Yang and T. Lian, *Nano Lett.*, 2013, **13**, 5255–5263.
132 T. Torimoto, H. Horibe, T. Kameyama, K.-i. Okazaki, S. Ikeda, M. Matsumura, A. Ishikawa and H. Ishihara, *J. Phys. Chem. Lett.*, 2011, **2**, 2057–2062.
133 G. Yu, X. Wang, J. Cao, S. Wu, W. Yan and G. Liu, *Chem. Commun.*, 2016, **52**, 2394–2397.
134 J. Li, S. K. Cushing, P. Zheng, T. Senty, F. Meng, A. D. Bristow, A. Manivannan and N. Wu, *J. Am. Chem. Soc.*, 2014, **136**, 8438–8449.
135 T. Peng, K. Li, P. Zeng, Q. Zhang and X. Zhang, *J. Phys. Chem. C*, 2012, **116**, 22720–22726.
136 J. Ge and Y. Li, *Adv. Funct. Mater.*, 2004, **14**, 157–162.
137 M. Muruganandham, Y. Kusumoto, C. Okamoto, A. Muruganandham, M. Abdulla-Al-Mamun and B. Ahmmad, *J. Phys. Chem. C*, 2009, **113**, 19506–19517.
138 J. Yang, J.-H. Zeng, S.-H. Yu, L. Yang, G.-e. Zhou and Y.-t. Qian, *Chem. Mater.*, 2000, **12**, 3259–3263.
139 H. Chu, X. Li, G. Chen, W. Zhou, Y. Zhang, Z. Jin, J. Xu and Y. Li, *Cryst. Growth Des.*, 2005, **5**, 1801–1806.
140 S. Kar, B. Satpati, P. Satyam and S. Chaudhuri, *J. Phys. Chem. B*, 2005, **109**, 19134–19138.
141 R. Thiruvengadathan and O. Regev, *Chem. Mater.*, 2005, **17**, 3281–3287.
142 W. Qingqing, X. Gang and H. Gaorong, *Cryst. Growth Des.*, 2006, **6**, 1776–1780.

143 N. Pinna, K. Weiss, J. Urban and M.-P. Pileni, *Adv. Mater.*, 2001, **13**, 261–264.
144 Y. Cheng, Y. Wang, F. Bao and D. Chen, *J. Phys. Chem. B*, 2006, **110**, 9448–9451.
145 L. Q. Pham, T.-K. Van, H. G. Cha and Y. S. Kang, *CrystEngComm*, 2012, **14**, 7888–7890.
146 L. Zhang, J. C. Yu, M. Mo, L. Wu, Q. Li and K. W. Kwong, *J. Am. Chem. Soc.*, 2004, **126**, 8116–8117.
147 P. Zhang and L. Gao, *J. Mater. Chem. A*, 2003, **13**, 2007–2010.
148 S. Xiong, B. Xi, C. Wang, G. Zou, L. Fei, W. Wang and Y. Qian, *Chem.–Eur. J.*, 2007, **13**, 3076–3081.
149 A. Phuruangrat, T. Thongtem and S. Thongtem, *Mater. Lett.*, 2009, **63**, 1538–1541.
150 Y. Guo, J. Wang, L. Yang, J. Zhang, K. Jiang, W. Li, L. Wang and L. Jiang, *CrystEngComm*, 2011, **13**, 5045–5048.
151 N. Bao, L. Shen, T. Takata and K. Domen, *Mater. Lett.*, 2007, **20**, 110–117.
152 Q. Wang, J. Lian, J. Li, R. Wang, H. Huang, B. Su and Z. Lei, *Sci. Rep.*, 2015, **5**, 1–9.
153 J. Yu, Y. Yu and B. Cheng, *RSC Adv.*, 2012, **2**, 11829–11835.
154 B. Zhang, W. Yao, C. Huang, Q. Xu and Q. Wu, *Int. J. Hydrogen Energy*, 2013, **38**, 7224–7231.
155 H.-C. Liao, S.-Y. Chen and D.-M. Liu, *Macromolecules*, 2009, **42**, 6558–6563.
156 W. Yao, X. Song, C. Huang, Q. Xu and Q. Wu, *Catal. Today*, 2013, **199**, 42–47.
157 Q. Wang, J. Li, N. An, Y. Bai, X. Lu, J. Li, H. Ma, R. Wang, F. Wang and Z. Lei, *Int. J. Hydrogen Energy*, 2013, **38**, 10761–10767.
158 I. Majeed, M. A. Nadeem, M. Al-Oufi, M. A. Nadeem, G. Waterhouse, A. Badshah, J. Metson and H. Idriss, *Appl. Catal., B*, 2016, **182**, 266–276.
159 X. Chen and W. Shangguan, *Front. Energy Res.*, 2013, **7**, 111.
160 S. Huang, Y. Lin, J.-H. Yang and Y. Yu, in *Nanotechnology for Sustainable Energy*, ACS Publications, 2013, pp. 219–241.
161 Y. Wang, Y. Wang and R. Xu, *J. Phys. Chem. C*, 2013, **117**, 783–790.
162 L. A. Silva, S. Y. Ryu, J. Choi, W. Choi and M. R. Hoffmann, *J. Phys. Chem. C*, 2008, **112**, 12069–12073.
163 H. Yan, J. Yang, G. Ma, G. Wu, X. Zong, Z. Lei, J. Shi and C. Li, *J. Catal.*, 2009, **266**, 165–168.
164 G. Xin, B. Yu, Y. Xia, T. Hu, L. Liu and C. Li, *J. Phys. Chem. C*, 2014, **118**, 21928–21934.
165 J. Jin, J. Yu, G. Liu and P. K. Wong, *J. Mater. Chem. A*, 2013, **1**, 10927–10934.
166 M. Luo, W. Yao, C. Huang, Q. Wu and Q. Xu, *J. Mater. Chem. A*, 2015, **3**, 13884–13891.
167 N. Sahu, S. Upadhyay and A. Sinha, *Int. J. Hydrogen Energy*, 2009, **34**, 130–137.
168 X. Zhou, H. Chen, Y. Sun, K. Zhang, X. Fan, Y. Zhu, Y. Chen, G. Tao and J. Shi, *Appl. Catal., B*, 2014, **152**, 271–279.
169 M. Sakamoto, A. Xiong, R. Kanakubo, T. Ikeda, T. Yoshinaga, K. Maeda, K. Domen and T. Teranishi, *Chem. Lett.*, 2012, **41**, 1325–1327.
170 S. Shen, L. Guo, X. Chen, F. Ren and S. S. Mao, *Int. J. Hydrogen Energy*, 2010, **35**, 7110–7115.
171 Y. Li, L. Tang, S. Peng, Z. Li and G. Lu, *CrystEngComm*, 2012, **14**, 6974–6982.
172 C. Janet and R. Viswanath, *Nanotechnology*, 2006, **17**, 5271.
173 Q. Wang, J. Li, N. An, Y. Bai, X. Lu, J. Li, H. Ma, R. Wang, F. Wang, Z. Lei and W. Shangguan, *Int. J. Hydrogen Energy*, 2013, **38**, 10761–10767.
174 W. Yao, C. Huang, N. Muradov and T. Ali, *Int. J. Hydrogen Energy*, 2011, **36**, 4710–4715.
175 M. Luo, W. Yao, C. Huang, Q. Wu and Q. Xu, *RSC Adv.*, 2015, **5**, 40892–40898.
176 Q. Chen, C. Suo, S. Zhang and Y. Wang, *Int. J. Photoenergy*, 2013, **1**, DOI: 10.1155/2013/149586.
177 X. Li, H. Liu, S. Liu, J. Zhang, W. Chen, C. Huang and L. Mao, *Int. J. Hydrogen Energy*, 2016, **41**, 23015–23021.
178 P. D. Cozzoli, T. Pellegrino and L. Manna, *Chem. Soc. Rev.*, 2006, **35**, 1195–1208.
179 W.-W. Zhao, J. Wang, J.-J. Xu and H.-Y. Chen, *Chem. Commun.*, 2011, **47**, 10990–10992.
180 X. Xing, R. Liu, X. Yu, G. Zhang, H. Cao, J. Yao, B. Ren, Z. Jiang and H. Zhao, *J. Mater. Chem. A*, 2013, **1**, 1488–1494.
181 Y. Shemesh, J. E. Macdonald, G. Menagen and U. Banin, *Angew. Chem.*, 2011, **123**, 1217–1221.
182 P. Kalisman, L. Houben, E. Aronovitch, Y. Kauffmann, M. Bar-Sadan and L. Amirav, *J. Mater. Chem. A*, 2015, **3**, 19679–19682.
183 Y. Du, B. Chen, Z. Yin, Z. Liu and H. Zhang, *Small*, 2014, **10**, 4727–4734.
184 H.-W. Tseng, M. B. Wilker, N. H. Damrauer and G. Dukovic, *J. Am. Chem. Soc.*, 2013, **135**, 3383–3386.
185 J. Ran, J. Yu and M. Jaroniec, *Green Chem.*, 2011, **13**, 2708–2713.
186 J. Zhang, S. Z. Qiao, L. Qi and J. Yu, *Phys. Chem. Chem. Phys.*, 2013, **15**, 12088–12094.
187 J. Meng, F. Li, Y. Hu, L. Xu, Z. Sun and J. Liu, *Mater. Res. Bull.*, 2013, **48**, 2111–2116.
188 W. Zhang, Y. Wang, Z. Wang, Z. Zhong and R. Xu, *Chem. Commun.*, 2010, **46**, 7631–7633.
189 T. Peng, X. Zhang, P. Zeng, K. Li, X. Zhang and X. Li, *J. Catal.*, 2013, **303**, 156–163.
190 X. Zong, H. Yan, G. Wu, G. Ma, F. Wen, L. Wang and C. Li, *J. Am. Chem. Soc.*, 2008, **130**, 7176–7177.
191 J. S. Jang, D. J. Ham, N. Lakshminarasimhan, W. y. Choi and J. S. Lee, *Appl. Catal., A*, 2008, **346**, 149–154.
192 L. Jia, D.-H. Wang, Y.-X. Huang, A.-W. Xu and H.-Q. Yu, *J. Phys. Chem. C*, 2011, **115**, 11466–11473.
193 Q. Li, B. Guo, J. Yu, J. Ran, B. Zhang, H. Yan and J. R. Gong, *J. Am. Chem. Soc.*, 2011, **133**, 10878–10884.
194 L. Jia, D.-H. Wang, Y.-X. Huang, A.-W. Xu and H.-Q. Yu, *J. Phys. Chem. C*, 2011, **115**, 11466–11473.
195 M. Liu, Y. Du, L. Ma, D. Jing and L. Guo, *Int. J. Hydrogen Energy*, 2012, **37**, 730–736.
196 J. Yang, H. Yan, X. Wang, F. Wen, Z. Wang, D. Fan, J. Shi and C. Li, *J. Catal.*, 2012, **290**, 151–157.
197 A. J. Frank, Z. Goren and I. Willner, *J. Chem. Soc., Chem. Commun.*, 1985, 1029–1030.
198 T. Peng, X. Zhang, P. Zeng, K. Li, X. Zhang and X. Li, *J. Catal.*, 2013, **303**, 156–163.

199 Q. Li, B. Guo, J. Yu, J. Ran, B. Zhang, H. Yan and J. R. Gong, *J. Am. Chem. Soc.*, 2011, **133**, 10878–10884.
200 Y.-P. Yuan, L.-W. Ruan, J. Barber, S. C. J. Loo and C. Xue, *Energy Environ. Sci.*, 2014, **7**, 3934–3951.
201 H. Chauhan, Y. Kumar, J. Dana, B. Satpati, H. N. Ghosh and S. Deka, *Nanoscale*, 2016, **8**, 15802–15812.
202 L. Chen, Y. Xu and B. Chen, *Appl. Catal., B*, 2019, **256**, 117848.
203 Y. Huang, J. Chen, W. Zou, L. Zhang, L. Hu, M. He, L. Gu, J. Deng and X. Xing, *Dalton Trans.*, 2016, **45**, 1160–1165.
204 Y. K. Kho, W. Y. Teoh, A. Iwase, L. Mädler, A. Kudo and R. Amal, *ACS Appl. Mater. Interfaces*, 2011, **3**, 1997–2004.
205 Y. Hou, F. Zuo, Q. Ma, C. Wang, L. Bartels and P. Feng, *J. Phys. Chem. C*, 2012, **116**, 20132–20139.
206 S. S. K. Ma, K. Maeda, T. Hisatomi, M. Tabata, A. Kudo and K. Domen, *Chem.–Eur. J.*, 2013, **19**, 7480–7486.
207 W.-T. Sun, Y. Yu, H.-Y. Pan, X.-F. Gao, Q. Chen and L.-M. Peng, *J. Am. Chem. Soc.*, 2008, **130**, 1124–1125.
208 H. Park, W. Choi and M. R. Hoffmann, *J. Mater. Chem.*, 2008, **18**, 2379–2385.
209 M. Moriya, T. Minegishi, H. Kumagai, M. Katayama, J. Kubota and K. Domen, *J. Am. Chem. Soc.*, 2013, **135**, 3733–3735.
210 J. Xu and X. Cao, *Chem. Eng. J.*, 2015, **260**, 642–648.
211 Y. Liu, Y.-X. Yu and W.-D. Zhang, *J. Phys. Chem. C*, 2013, **117**, 12949–12957.
212 S. Liang, Z. Zhou, X. Wu, S. Zhu, J. Bi, L. Zhou, M. Liu and L. Wu, *Molecules*, 2016, **21**, 213.
213 S. Ma, J. Xie, J. Wen, K. He, X. Li, W. Liu and X. Zhang, *Appl. Surf. Sci.*, 2017, **391**, 580–591.
214 D. Jiang, Z. Sun, H. Jia, D. Lu and P. Du, *J. Mater. Chem. A*, 2016, **4**, 675–683.
215 J. Zhang, L. Wang, X. Liu, X. a. Li and W. Huang, *J. Mater. Chem. A*, 2015, **3**, 535–541.
216 J. Zhang, Y. Wang, J. Zhang, Z. Lin, F. Huang and J. Yu, *ACS Appl. Mater. Interfaces*, 2013, **5**, 1031–1037.
217 C. W. Raubach, Y. V. de Santana, M. M. Ferrer, V. M. Longo, J. A. Varela, W. Avansi, P. G. Buzolin, J. R. Sambrano and E. Longo, *Chem. Phys. Lett.*, 2012, **536**, 96–99.
218 Y. P. Xie, Z. B. Yu, G. Liu, X. L. Ma and H.-M. Cheng, *Energy Environ. Sci.*, 2014, **7**, 1895–1901.
219 T. T. Zhuang, Y. Liu, M. Sun, S. L. Jiang, M. W. Zhang, X. C. Wang, Q. Zhang, J. Jiang and S. H. Yu, *Angew. Chem.*, 2015, **127**, 11657–11662.
220 Y. Li, X. Wei, H. Li, R. Wang, J. Feng, H. Yun and A. Zhou, *RSC Adv.*, 2015, **5**, 14074–14080.
221 J. Liu, *J. Phys. Chem. C*, 2015, **119**, 28417–28423.
222 Z. Xu, H. Li, Z. Wu, J. Sun, Z. Ying, J. Wu and N. Xu, *J. Phys. Chem. C*, 2016, **4**, 7501–7507.
223 J. Zhang, Y. Wang, J. Jin, J. Zhang, Z. Lin, F. Huang and J. Yu, *ACS Appl. Mater. Interfaces*, 2013, **5**, 10317–10324.
224 L. Ge, F. Zuo, J. Liu, Q. Ma, C. Wang, D. Sun, L. Bartels and P. Feng, *J. Phys. Chem. C*, 2012, **116**, 13708–13714.
225 S. Chaguetmi, F. Mammeri, M. Pasut, S. Nowak, H. Lecoq, P. Decorse, C. Costentin, S. Achour and S. Ammar, *J. Nanopart. Res.*, 2013, **15**, 2140.
226 Y. Yin, Z. Jin and F. Hou, *Nanotechnology*, 2007, **18**, 495608.
227 H. B. Yang, J. Miao, S.-F. Hung, F. Huo, H. M. Chen and B. Liu, *ACS Nano*, 2014, **8**, 10403–10413.
228 T. Jafari, E. Moharreri, A. S. Amin, R. Miao, W. Song and S. L. Suib, *Molecules*, 2016, **21**, 900.
229 Y. Li, L. Zhang, W. Wu, P. Dai, X. Yu, M. Wu and G. Li, *Nanoscale Res. Lett.*, 2014, **9**, 270.
230 P. Lv, W. Fu, H. Yang, H. Sun, Y. Chen, J. Ma, X. Zhou, L. Tian, W. Zhang and M. Li, *CrystEngComm*, 2013, **15**, 7548–7555.
231 S. T. Kochuveedu, *J. Nanomater.*, 2016, **2016**, 12.
232 Y.-Y. Hsu, N.-T. Suen, C.-C. Chang, S.-F. Hung, C.-L. Chen, T.-S. Chan, C.-L. Dong, C.-C. Chan, S.-Y. Chen and H. M. Chen, *ACS Appl. Mater. Interfaces*, 2015, **7**, 22558–22569.
233 K. Li, M. Han, R. Chen, S. L. Li, S. L. Xie, C. Mao, X. Bu, X. L. Cao, L. Z. Dong and P. Feng, *Adv. Mater.*, 2016, **28**, 8906–8911.
234 Y. Huang, J. Chen, W. Zou, L. Zhang, L. Hu, M. He, L. Gu, J. Deng and X. Xing, *Dalton Trans.*, 2016, **45**, 1160–1165.
235 K. Li, M. Han, R. Chen, S. L. Li, S. L. Xie, C. Mao, X. Bu, X. L. Cao, L. Z. Dong and P. Feng, *Adv. Mater.*, 2016, **28**, 8906–8911.
236 S. Cao, Y. Chen, L. Kang, Z. Lin and W.-F. Fu, *J. Mater. Chem.*, 2015, **3**, 18711–18717.
237 J. Song, H. Zhao, R. Sun, X. Li and D. Sun, *Energy Environ. Sci.*, 2017, **10**, 225–235.
238 Y. Zhong, Y. Shao, F. Ma, Y. Wu, B. Huang and X. Hao, *Nano Energy*, 2017, **31**, 84–89.
239 Z. Lin, L. Li, L. Yu, W. Li and G. Yang, *J. Mater. Chem. A*, 2017, **5**, 5235–5259.
240 W. Jiang, Y. Liu, R. Zong, Z. Li, W. Yao and Y. Zhu, *J. Mater. Chem. A*, 2015, **3**, 18406–18412.
241 Y.-X. Yu, W.-X. Ouyang, Z.-T. Liao, B.-B. Du and W.-D. Zhang, *ACS Appl. Mater. Interfaces*, 2014, **6**, 8467–8474.
242 X. Wang, C. Liow, D. Qi, B. Zhu, W. R. Leow, H. Wang, C. Xue, X. Chen and S. Li, *Adv. Mater.*, 2014, **26**, 3506–3512.
243 J. U. Bang, S. J. Lee, J. S. Jang, W. Choi and H. Song, *J. Phys. Chem. Lett.*, 2012, **3**, 3781–3785.
244 P. Tongying, F. Vietmeyer, D. Aleksiuk, G. Ferraudi, G. Krylova and M. Kuno, *Nanoscale*, 2014, **6**, 4117–4124.
245 X. Zong, J. Han, G. Ma, H. Yan, G. Wu and C. Li, *J. Phys. Chem. C*, 2011, **115**, 12202–12208.
246 K. Iwashina, A. Iwase, Y. H. Ng, R. Amal and A. Kudo, *J. Am. Chem. Soc.*, 2015, **137**, 604–607.
247 W.-K. Jo and N. C. S. Selvam, *Chem. Eng. J.*, 2017, **317**, 913–924.
248 Y. Huang, Y. Liu, D. Zhu, Y. Xin and B. Zhang, *J. Mater. Chem. A*, 2016, **4**, 13626–13635.
249 H. Tada, T. Mitsui, T. Kiyonaga, T. Akita and K. Tanaka, *Nat. Mater.*, 2006, **5**, 782–786.
250 Y. Nosaka, *J. Phys. Chem.*, 1991, **95**, 5054–5058.
251 J. S. Jang, U. A. Joshi and J. S. Lee, *J. Phys. Chem. C*, 2007, **111**, 13280–13287.
252 J. S. Jang, D. J. Ham, N. Lakshminarasimhan, W. y. Choi and J. S. Lee, *Appl. Catal., A*, 2008, **346**, 149–154.

253 N. Bao, L. Shen, T. Takata, K. Domen, A. Gupta, K. Yanagisawa and C. A. Grimes, *J. Phys. Chem. C*, 2007, **111**, 17527–17534.
254 N. Bao, L. Shen, T. Takata and K. Domen, *Chem. Mater.*, 2007, **20**, 110–117.
255 M. Sathish and R. Viswanath, *Catal. Today*, 2007, **129**, 421–427.
256 M. Muruganandham, Y. Kusumoto, C. Okamoto, A. Muruganandham, M. Abdulla-Al-Mamun and B. Ahmmad, *J. Phys. Chem. C*, 2009, **113**, 19506–19517.
257 A. Deshpande, P. Shah, R. Gholap and N. M. Gupta, *J. Colloid Interface Sci.*, 2009, **333**, 263–268.
258 G. De, A. Roy and S. Bhattacharya, *Int. J. Hydrogen Energy*, 1995, **20**, 127–131.
259 J. Zhang, J. Yu, M. Jaroniec and J. R. Gong, *Nano Lett.*, 2012, **12**, 4584–4589.
260 Z. Shen, G. Chen, Q. Wang, Y. Yu, C. Zhou and Y. Wang, *Nanoscale*, 2012, **4**, 2010–2017.
261 J. Yang, H. Yan, X. Wang, F. Wen, Z. Wang, D. Fan, J. Shi and C. Li, *J. Catal.*, 2012, **290**, 151–157.
262 S. Shen, L. Guo, X. Chen, F. Ren and S. S. Mao, *Int. J. Hydrogen Energy*, 2010, **35**, 7110–7115.
263 A. Ye, W. Fan, Q. Zhang, W. Deng and Y. Wang, *Catal. Sci. Technol.*, 2012, **2**, 969–978.
264 J. Zhang, J. Yu, M. Jaroniec and J. R. Gong, *Nano Lett.*, 2012, **12**, 4584–4589.
265 D. He, M. Chen, F. Teng, G. Li, H. Shi, J. Wang, M. Xu, T. Lu, X. Ji and Y. Lv, *Superlattices Microstruct.*, 2012, **51**, 799–808.
266 H. Park, W. Choi and M. R. Hoffmann, *J. Mater. Chem. A*, 2008, **18**, 2379–2385.
267 J. S. Jang, H. G. Kim, U. A. Joshi, J. W. Jang and J. S. Lee, *Int. J. Hydrogen Energy*, 2008, **33**, 5975–5980.
268 S. Zhang, Q. Chen, D. Jing, Y. Wang and L. Guo, *Int. J. Hydrogen Energy*, 2012, **37**, 791–796.
269 J. Hou, Z. Wang, W. Kan, S. Jiao, H. Zhu and R. Kumar, *J. Mater. Chem. A*, 2012, **22**, 7291–7299.
270 Y. Chen, L. Wang, G. M. Lu, X. Yao and L. Guo, *J. Mater. Chem.*, 2011, **21**, 5134–5141.
271 T. Peng, P. Zeng, D. Ke, X. Liu and X. Zhang, *Energy Fuels*, 2011, **25**, 2203–2210.
272 T. Kida, G. Guan and A. Yoshida, *Chem. Phys. Lett.*, 2003, **371**, 563–567.
273 D. Ke, S. Liu, K. Dai, J. Zhou, L. Zhang and T. Peng, *J. Phys. Chem. C*, 2009, **113**, 16021–16026.
274 L. Wang and W. Wang, *CrystEngComm*, 2012, **14**, 3315–3320.
275 X. Wang, G. Liu, G. Q. Lu and H.-M. Cheng, *Int. J. Hydrogen Energy*, 2010, **35**, 8199–8205.
276 L. Xu, W. Shi and J. Guan, *Catal. Commun.*, 2012, **25**, 54–58.
277 X.-H. Lu, S.-L. Xie, T. Zhai, Y.-F. Zhao, P. Zhang, Y.-L. Zhang and Y.-X. Tong, *RSC Adv.*, 2011, **1**, 1207–1210.
278 X. Wang, G. Liu, L. Wang, Z. G. Chen, G. Q. M. Lu and H. M. Cheng, *Adv. Energy Mater.*, 2012, **2**, 42–46.
279 Z. Khan, M. Khannam, N. Vinothkumar, M. De and M. Qureshi, *J. Mater. Chem.*, 2012, **22**, 12090–12095.
280 X. Wang, G. Liu, G. Q. Lu and H.-M. Cheng, *Int. J. Hydrogen Energy*, 2010, **35**, 8199–8205.
281 J. Ran, J. Yu and M. Jaroniec, *Green Chem.*, 2011, **13**, 2708–2713.
282 J. Hou, Z. Wang, W. Kan, S. Jiao, H. Zhu and R. Kumar, *J. Mater. Chem.*, 2012, **22**, 7291–7299.
283 X. Ding, Y. Li, J. Zhao, Y. Zhu, Y. Li, W. Deng and C. Wang, *APL Mater.*, 2015, **3**, 104410.
284 J. Chen, X. J. Wu, L. Yin, B. Li, X. Hong, Z. Fan, B. Chen, C. Xue and H. Zhang, *Angew. Chem., Int. Ed.*, 2015, **54**, 1210–1214.
285 X. Chen, W. Chen, H. Gao, Y. Yang and W. Shangguan, *Appl. Catal., B*, 2014, **152**, 68–72.
286 L. J. Zhang, T. F. Xie, D. J. Wang, S. Li, L. L. Wang, L. P. Chen and Y. C. Lu, *Int. J. Hydrogen Energy*, 2013, **38**, 11811–11817.
287 J. Zhang, S. Z. Qiao, L. Qi and J. Yu, *Phys. Chem. Chem. Phys.*, 2013, **15**, 12088–12094.
288 E. Baniasadi, I. Dincer and G. Naterer, *Appl. Catal., A*, 2013, **455**, 25–31.
289 L. J. Zhang, R. Zheng, S. Li, B. K. Liu, D. J. Wang, L. L. Wang and T. F. Xie, *ACS Appl. Mater. Interfaces*, 2014, **6**, 13406–13412.
290 H. Wang, W. Chen, J. Zhang, C. Huang and L. Mao, *Int. J. Hydrogen Energy*, 2015, **40**, 340–345.
291 X. Wang, M. Liu, Q. Chen, K. Zhang, J. Chen, M. Wang, P. Guo and L. Guo, *Int. J. Hydrogen Energy*, 2013, **38**, 13091–13096.
292 N. Biswal, D. Das, S. Martha and K. Parida, *Int. J. Hydrogen Energy*, 2011, **36**, 13452–13460.
293 E. Hong, D. Kim and J. H. Kim, *Ind. Eng. Chem. Res.*, 2014, **20**, 3869–3874.
294 Q. Li, B. Guo, J. Yu, J. Ran, B. Zhang, H. Yan and J. R. Gong, *J. Am. Chem. Soc.*, 2011, **133**, 10878–10884.
295 Z. Yan, Z. Sun, X. Liu, H. Jia and P. Du, *Nanoscale*, 2016, **8**, 4748–4756.
296 J. J. Wang, Z. J. Li, X. B. Li, X. B. Fan, Q. Y. Meng, S. Yu, C. B. Li, J. X. Li, C. H. Tung and L. Z. Wu, *ChemSusChem*, 2014, **7**, 1468–1475.
297 Y. X. Pan, H. Zhuang, J. Hong, Z. Fang, H. Liu, B. Liu, Y. Huang and R. Xu, *ChemSusChem*, 2014, **7**, 2537–2544.
298 P. S. Lunawat, R. Kumar and N. M. Gupta, *Catal. Lett.*, 2008, **121**, 226–233.
299 P. S. Lunawat, S. Senapati, R. Kumar and N. M. Gupta, *Int. J. Hydrogen Energy*, 2007, **32**, 2784–2790.
300 J. Thote, H. B. Aiyappa, A. Deshpande, D. Díaz Díaz, S. Kurungot and R. Banerjee, *Chem.–Eur. J.*, 2014, **20**, 15961–15965.
301 M. B. Wilker, J. K. Utterback, S. Greene, K. A. Brown, D. W. Mulder, P. W. King and G. Dukovic, *J. Phys. Chem. C*, 2018, **122**, 741–750.
302 Y. Lin, J. Zhang, E. Sargent and E. Kumacheva, *Appl. Phys. Lett.*, 2002, **81**, 3134–3136.
303 E. Hong, D. Kim and J. H. Kim, *J. Ind. Eng. Chem.*, 2014, **20**, 3869–3874.
304 N. Buehler, K. Meier and J. F. Reber, *J. Phys. Chem.*, 1984, **88**, 3261–3268.
305 J. Schneider and D. W. Bahnemann, *J. Phys. Chem. Lett.*, 2013, **4**, 3479–3483.

306 X. Chen, S. Shen, L. Guo and S. S. Mao, *Chem. Rev.*, 2010, **110**, 6503–6570.
307 K. Maeda and K. Domen, *J. Phys. Chem. C*, 2007, **111**, 7851–7861.
308 A. Kudo, *Int. J. Hydrogen Energy*, 2006, **31**, 197–202.
309 T. Kawai and T. Sakata, *J. Chem. Soc., Chem. Commun.*, 1980, 694–695.
310 M. J. Berr, P. Wagner, S. Fischbach, A. Vaneski, J. Schneider, A. S. Susha, A. L. Rogach, F. Jäckel and J. Feldmann, *Appl. Phys. Lett.*, 2012, **100**, 223903.
311 H. Harada, T. Sakata and T. Ueda, *J. Am. Chem. Soc.*, 1985, **107**, 1773–1774.
312 X. Zong, G. Wu, H. Yan, G. Ma, J. Shi, F. Wen, L. Wang and C. Li, *J. Phys. Chem. C*, 2010, **114**, 1963–1968.
313 T. Peng, K. Li, P. Zeng, Q. Zhang and X. Zhang, *J. Phys. Chem. C*, 2012, **116**, 22720–22726.
314 S. Shen and L. Guo, *Mater. Res. Bull.*, 2008, **43**, 437–446.
315 W. Yao, X. Song, C. Huang, Q. Xu and Q. Wu, *Catal. Today*, 2013, **199**, 42–47.
316 D. Ke, S. Liu, K. Dai, J. Zhou, L. Zhang and T. Peng, *J. Phys. Chem. C*, 2009, **113**, 16021–16026.
317 S. Chen and L.-W. Wang, *Chem. Mater.*, 2012, **24**, 3659–3666.
318 H. Yan, J. Yang, G. Ma, G. Wu, X. Zong, Z. Lei, J. Shi and C. Li, *J. Catal.*, 2009, **266**, 165–168.
319 M. J. Berr, A. Vaneski, C. Mauser, S. Fischbach, A. S. Susha, A. L. Rogach, F. Jäckel and J. Feldmann, *Small*, 2012, **8**, 291–297.
320 X. Chen, S. Shen, L. Guo and S. S. Mao, *Chem. Rev.*, 2010, **110**, 6503–6570.
321 A. B. Ellis, S. W. Kaiser, J. M. Bolts and M. S. Wrighton, *J. Am. Chem. Soc.*, 1977, **99**, 2839–2848.
322 H. Fujiwara, H. Hosokawa, K. Murakoshi, Y. Wada, S. Yanagida, T. Okada and H. Kobayashi, *J. Phys. Chem. B*, 1997, **101**, 8270–8278.
323 N. S. Lewis, *Nature*, 2001, **414**, 589.
324 K. Sanderson, *Nature*, 2008, **452**, 400–402.